MICROCOPY RESOLUTION TEST CHART
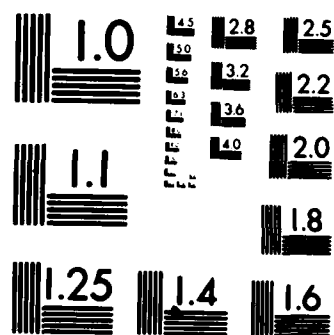NATIONAL BUREAU OF STANDARDS-1963-A

REPORT DOCUMENTATION PAGE

1a. REPORT SECURITY CLASSIFICATION	1b. RESTRICTIVE MARKINGS
UNCALSSIFIED	

2a. SECURITY CLASSIFICATION AUTHORITY	3. DISTRIBUTION/AVAILABILITY OF REPORT
	Approved for public release;
2b. DECLASSIFICATION/DOWNGRADING SCHEDULE	distribution unlimited

4. PERFORMING ORGANIZATION REPORT NUMBER(S)	5. MONITORING ORGANIZATION REPORT NUMBER(S)
AD-A170 653	AFOSR·TR· 86 - 0 5 6 8

6a. NAME OF PERFORMING ORGANIZATION	6b. OFFICE SYMBOL (If applicable)	7a. NAME OF MONITORING ORGANIZATION
Stanford University	NP	AFOSR/NP

6c. ADDRESS (City, State and ZIP Code)	7b. ADDRESS (City, State and ZIP Code)
Edward L. Ginzton Laboratory for Physics Stanford, CA 94305	Building 410 Bolling AFB D C 20332-6448

8a. NAME OF FUNDING/SPONSORING ORGANIZATION	8b. OFFICE SYMBOL (If applicable)	9. PROCUREMENT INSTRUMENT IDENTIFICATION NUMBER
AFOSR	NP	F49620-84-C-0021

8c. ADDRESS (City, State and ZIP Code)	10. SOURCE OF FUNDING NOS.			
Building 410 Bolling AFB DC 20332-6448	PROGRAM ELEMENT NO.	PROJECT NO.	TASK NO.	WORK UNIT NO.
	61102F	2301	A1	N/A

11. TITLE (Include Security Classification)
LASER PHYSICS AND LASER SPECTROSCOPY

12. PERSONAL AUTHOR(S)
Dr. Robert L. Byer

13a. TYPE OF REPORT	13b. TIME COVERED	14. DATE OF REPORT (Yr., Mo., Day)	15. PAGE COUNT
Final	FROM 15 Feb 84 TO 14 Feb 85	86 Mar 01	44

16. SUPPLEMENTARY NOTATION

17.	COSATI CODES		18. SUBJECT TERMS (Continue on reverse if necessary and identify by block number)
FIELD	GROUP	SUB. GR.	

19. ABSTRACT (Continue on reverse if necessary and identify by block number) In its second year of operation, the single crystal fiber growth machine has produced over 400 fibers of a variety of materials, some of which had never before been grown in fiber form. A high speed, high resolution, long working distance diameter measurement system has been constructed and installed on the growth machine. It has enabled the closed-loop growth of single crystal fibers possessing diameter stability a factor of four better than the fibers grown without feedback diameter control. the first monolithic single crystal fiber devices, a fiber ruby laser and a sapphire fiber thermometer, have been studied.

DTIC FILE COPY

DTIC
ELECTE
AUG 1 1 1986
S D

20. DISTRIBUTION/AVAILABILITY OF ABSTRACT	21. ABSTRACT SECURITY CLASSIFICATION
UNCLASSIFIED/UNLIMITED ☒ SAME AS RPT. ☐ DTIC USERS ☐	UNCLASSIFIED

22a. NAME OF RESPONSIBLE INDIVIDUAL	22b. TELEPHONE NUMBER (Include Area Code)	22c. OFFICE SYMBOL
Dr Howard R Schlossberg	202/767-4906	NP

Edward L. Ginzton Laboratory of Physics
Stanford University
Stanford, California 94305

AFOSR·TR· 86 - 0 5 68

LASER PHYSICS AND LASER SPECTROSCOPY

Final Technical Report

for

Air Force Office of Scientific Research
Contract number: F49620-84-C-0021

for the period

February 15, 1984 to February 14, 1985

Principal Investigator

Robert L. Byer

G.L. Number:

March 1985

TABLE OF CONTENTS

Distribution/

Availability Codes

Dist	Avail and/or Special
A-1	

LASER PHYSICS AND LASER SPECTROSCOPY
Robert L. Byer

I.   INTRODUCTION

The growth of crystalline materials in fiber optical
form makes possible a variety of devices which will be
useful in the generation and processing of light and which
will couple well to glass fibers used for transmission.
Optical fibers can be made from materials which can withstand
more adverse conditions than glass fibers. Nonlinear optical
processes can operate more efficiently in a waveguide because
confinement provides high optical intensities over long inter-
action lengths, a combination which is not available in bulk
crystals due to diffraction. Crystalline lasers and modulators
can be made, as well as passive components such as polarizers,
isolators and filters.

Crystalline fibers are grown at Stanford using the laser
heated miniature pedestal growth technique. In this crucible-less
method, a CO_2 laser melts the end of a rod of feed material.
A seed crystal is then dipped into the molten zone thus formed
and the fiber is grown by pulling the seed away from the melt
while fresh feed material is simultaneously fed into the molten zone.
A diameter reduction is obtained by pulling the seed more rapidly
than the source is fed in. Since this is a freezing process,

and not a stretching process as in the drawing of glass fibers, fluctuations in the diameter of the freezing interface are literally frozen into the as-grown fiber.

We have concentrated on the materials sapphire Al_2O_3, ruby $Cr:Al_2O_3$, Nd:YAG and $LiNbO_3$. Sapphire is useful for passive components, high power carrying capability and its resisitance to corrosive and high temperature environments. Ruby and Nd:YAG are laser materials, and $LiNbO_3$ is of great interest in nonlinear optical applications.

In all these applications, it is necessary to grow smooth fibers with minimal fluctuations in diameter. Diameter ripples on the order of a few percent of the mean diameter can cause the loss of light out of the fiber by scattering. Diameter fluctuations on the order of a few tenths of a percent can cause reduction in the efficiency of nonlinear interactions because, while scattering out of the fiber and into "radiation modes" may be small, fluctuations of this size can scatter light between guided modes. Light lost into the wrong guided mode is then unavailable because it does not meet the phase-matching requirement of the nonlinear interaction. As a result, a major thrust of our effort has been in the improvement of the diameter stability of the fibers.

Besides growing fibers of materials of interest, other steps must be accomplished before useful devices can be obtained. It must be possible to put optically polished ends on the fibers.

Ferroelectric materials must be "poled", or made to contain
a single domain or other desirable domain structure. A method
for cladding the fibers must be found to reduce the core size
and protect the refractive index interface. Methods must be
found to characterize the performance of fibers and the devices
made from them. Our reserach program addresses all these issues,
and significant progress has been made on every front in the
past year.

Investigation of the vacuum ultraviolet spectroscopy of
ionized indium vapor was motivated by interest in extending
the operating range of re-combination lasers to vacuum ultra-
violet. It is planned to use broad bandwidth ionizing radiation
in the soft X-ray region to preferentially remove inner shell
electrons from indium ions in the ground state. When these
electrons re-combine they initially occupy outer shell positions
leaving the inner shell electron vacancies. In this way we
propose to produce a population inversion in doubly ionized
indium for a transition at 185 nm.

In preliminary experiments, a pulsed carbon dioxide laser
was used to evaporate a plume of indium vapor from a molten pool
of the metal. A Q-switched Nd:YAG laser doubled to the green
is now being used for this purpose. A second Nd:YAG pulse is
used to produce the broad band ionizing radiation by creating
a plasma at the surface of a high atomic number metal target.
In an initial step the broad band radiation has been used to
characterize the laser produced indium plasma. It was found

that there is a large ground state population singly ionized indium in the evaporated plume. This is a required initial condition to proceed with pumping the laser transition.

II. PROGRESS IN SINGLE CRYSTAL FIBER RESEARCH

In the past year nearly 400 fibers have been grown of sapphire, ruby, Nd:YAG and LiNbO$_3$. The growth station has proven to be straightforward to operate and currently eleven students in three different research groups are qualified to grow fibers. In attition to the "traditional" materials listed above, several new materials have been grown. These include titanium-doped sapphire (Ti:Al$_2$O$_3$), a tunable laser material; magnesium-doped lithium niobate (Mg:LiNbO$_3$), which has the advantage of a higher resistance to photorefractive damage, a scattering effect which limits the power throughout of a device; terbium gallium garnet (TGG), a Faraday isolator material; potassium niobate (KNbO$_3$) a nonlinear material useful for near-room temperature frequency doubling the light from GaAs diode lasers into the blue; and Nd:LiNbO$_3$, a laser material which could internally double its own light. Studies have also been made on doping the end of sapphire fibers with Fe, Cu, Ni and Cr to form black-body radiators for use in a sapphire fiber thermometer.

In the fabrication field, new jigs made of the same crystalline material as the fiber have been made to hold fibers during the polishing operation. This allows the end faces to be polished flat and perpendicular to the fiber axis. The jig uses evaporated gold layers to cushion the clamping action on the fiber. These tools have proven especially important in the fabrication of fiber lasers.

- 4 -

An idea for accomplishing the poling of $LiNbO_3$ fibers with the application of thermal gradients has been proposed based on evidence obtained during fiber growth. A domain wall has been moved appreciably with this technique, and it nears further experimentation. Studies characterizing the formation of claddings and waveguides by diffusing protons from an acid bath into $LiNbO_3$ have been accepted for publication in Optics Letters and presentation at C.L.E.O.'85. These studies have been performed largely on plates of $LiNbO_3$, forming slab waveguides, but the results are applicable to the fiber geometry.

A diameter measurement system with 0.01% diameter resolution, 6 μm axial resolution, 160 mm working distance and a 1 kHz measurement rate has been constructed and installed in the growth station. Closed loop control of the fiber diameter has been accomplished using a simple analog proportional controller. Already a factor of 4 improvement in diameter stability over the best open loop growth has been seen.

Measurements are underway to determine the effects of perturbations in growth conditions on the fiber diameter, as well as to identify the sources of existing perturbations. Knowledge of the growth process transfer functions will enable us to design more effective control systems for stabilizing the fiber diameter to within our goal of 0.1%. A paper on the controlled growth of fibers will be presented at C.L.E.O.'85.

The first real monolithic single crystal fiber device, a liquid nitrogen cooled fiber ruby laser, has been demonstrated. A paper on this device has been submitted to Applied Physics Letters and a poster paper will be presented on it at C.L.E.O.'85. Further work will be performed on monolithic Nd:YAG fiber lasers. Second harmonic generation has also been performed, albeit unguided, in $LiNbO_3$ fibers. Tests are also underway on the sapphire fiber thermometer to determine its lifetime, spectral "blackness", and the amount of undesirable background radiation emitted by the sapphire itself.

III. PROGRESS ON INDIUM PHOTOIONIZATION LASER

In the past year we have demonstrated that extremely large densities of ground state indium ions (singly ionized), can be produced by laser ablation. Using only 100 milli-joules of 532 nm Q-switched light from a Nd:YAG laser, we have produced densitites $10^{15} - 10^{17}$ per cubic centimeter of ground state In II lasting for several hundred nanoseconds. These densities are of the order needed for the production of an indium photo-ionization pumped laser. The density measurements are by the "curve of growth" method, described below.

February to May of 1984 was spent refurbishing a surplus vacuum spectrometer and building a diffusion pumping station for it. The vacuum spectrometer enabled us to observe self-reversal on the 1586.4 angstrom resonance line of In II, seen in the recombination radiation as the laser ablated indium plasma cooled. This self-reversal was our first evidence of large populations of indium due to laser ablation. Observation of

- 6 -

different wavelengths of recombination radiation in different spatial regions of the indium plasma continued through September 1984, allowing us to plan changes in equipment and techniques needed to carry on the experiments.

October through December was spent improving equipment. The signal-to-noise ratio of the system was improved several orders of magnitude, allowing spectral measurements to be made with resolutions of 0.2 angstrom at 1586.4 angstroms. This was necessary to carry out the curve-of-growth measurements of ion density, and other characterizations of the indium plasma. Improvements were also made to the molten indium target boat, allowing better control of its temperature and allowing the target to be moved relative to the axis of observation. Also, a small absorption vacuum pump was added to the glass cell containing the indium plasma, reducing interference from atmospheric gases which leak into the cell.

With these improvements, successful curve-of-growth measurements of ion density followed in January and February 1985. The curve-of-growth technique involves measuring the absorption of light passing through the indium plasma as a function of wavelength. We have used a laser produced plasma as the broad band vacuum ultraviolet light source for these measurements.

The uncertainty in the ground state In II densities quoted in the first paragraph is due to line broadening of the absorption transition being observed. The broadening mechanisms

include Stark broadening by electron impact and by collisions with other ions, as well as resonance broadening by other ions of the same species and pressure broadening by the background helium pressure in the cell. The broadening due to these mechanisms will be calculated in the future, allowing accurate calculations of ion densities to be made.

In the near future we plan to make time resolved density measurements for several electron states in neutral indium and the first two ion stages. This will allow us to compute the plasma temperature and electron density as a function of time in the indium plasma. With this information we can choose the proper position and time in the plasma to apply the photo-ionization pump needed to produce a laser at 1850 angstroms.

IV. PUBLICATIONS AND PRESENTATIONS

1. R.L. Byer, K. Kuhn, M. Reed and J. Trail, "Progress in High Peak and Average Power Lasers for Soft X-ray Production", S.P.I.E. Proc., vol. 448, in X-ray Lithography and Applications of Soft X-rays to Technology, p.2, 1984.

2. K. Bennett and R.L. Byer, "Optical Tomography : Noise Theory and Experiment", Optics Letters, vol. 9, July 1984.

3. K.E. Bennett, G.W. Faris and R.L. Byer, "Experimental Optical Fan Beam Tomography", Applied Optics, vol. 23, p. 2678 – 2685, August 15th 1984.

4. M. Fejer, J. Nightingale, G. Magel and R.L. Byer, "Laser Assisted Growth of Optical Quality Single Crystal Fibers", S.P.I.E. Proc., vol. 460, Processing of Guided Wave Opto-electronic Materials, p.26 – 31, 1984.

5. M. Fejer, J. Nightingale, G. Magel and R.L. Byer, "Laser Heated Miniature Pedestal Growth Apparatus for Single Crystal Optical Fibers", Rev. Sci. Instr. vol. 55, p.1791 – 1796, 1984.

6. M. Digonnet, M. Fejer and R.L. Byer, "Characterization of Proton Exchanged Waveguides in $MgO : LiNbO_3$", accepted for publication in Optics Letters.

7. K. Bennett and R.L. Byer, "Fan Beam Tomography Noise Theory", submitted to J. Op. Soc. Am. <u>A</u>.

8. J.L. Nightingale and R.L. Byer, "A Guided Wave Monolithic Resonant Ruby Fiber Laser", submitted to Appl. Phys. Letts.

9. M.M. Fejer, G.A. Magel and R.L. Byer, "High Speed, High Resolution Fiber Diameter Measurement System", submitted to Applied Optics.

INVITED PRESENTATIONS

1. R.L. Byer, "Single Crystal Fibers", invited paper, Japanese Opto-electronic Association Meeting, Tokyo, Japan, January 1985.

CONTRIBUTED PRESENTATIONS

1. M.M. Fejer, J.L. Nightingale, G.A. Magel, T.Y. Fan, W. Kozlovsky and R.L. Byer, "Single Crystal Optical Fibers : Growth and Applications", paper ThI12, presented at the Conference on Lasers and Electro-optics, Anaheim, California, June 19th,1984.

2. K. Bennett, G.W. Faris and R.L. Byer, "Experimental Optical Tomography", paper WJ5, presented at the Conference on Lasers and Electro-optics, Anaheim, California, June 19th, 1984.

3. M. Fejer, J. Nightingale, G. Magel, W. Kozlovsky, T.Y. Fan and R.L. Byer, "Nonlinear Interactions in Single Crystal Fibers", N.A.S.A. Workshop on Tunable Solid State Lasers for Remote Sensing, Menlo Park, California, October 1st, 1984.

4. R.L. Byer, "Single Crystal Fiber Research", University of Osaka, Osaka, Japan, January 30th, 1985.

5. G.A. Magel, M.M. Fejer, J.L. Nightingale and R.L. Byer, "Controlled Growth of Single Crystal Optical Fibers", submitted for presentation at the Conference on Lasers and Electro-optics, Baltimore, May 21st, 1985.

6. J.L. Nightingale and R.L. Byer, "Monolithic Resonator Single Crystal Fiber Laser", submitted for presentation at the Conference on Lasers and Electro-optics, Baltimore, Maryland, May 21st, 1985.

7. M. Digonnet, M. Fejer and R.L. Byer, "Proton Exchange Waveguides in $MgO : LiNbO_3$", accepted for presentation at The Conference on Lasers and Electro-optics, Baltimore, Maryland, May 21st, 1985.

8. G.W. Faris and R.L. Byer, "Tomographic Imaging of a Supersonic Jet", accepted for presentation at the Conference on Lasers and Electro-optics, Baltimore, Maryland, May 21st, 1985.

V. PROFESSIONAL PERSONNEL ASSOCIATED WITH THE PROGRAM

Principal Investigator: Robert L. Byer
Professor of Applied Physics

Senior Research Associate: Robert Eckardt

Graduate Students:

Robert	Lacy
Marty	Fejer
John	Nightingale
Greg	Magel
William	Kozlovsky
Tso Yee	Fan
Keith	Bennett - Ph.D. awarded 1984

Laser-heated miniature pedestal growth apparatus for single-crystal optical fibers

M. M. Fejer, J. L. Nightingale, G. A. Magel, and R. L. Byer

Applied Physics Department, Edward L. Ginzton Laboratory of Physics, Stanford University, Stanford, California 94305

We have designed and built a single-crystal fiber growth apparatus. The apparatus employs novel optical, mechanical, and electronic control systems that enable the growth of high optical quality single-crystal fibers. We have grown oriented single-crystal fibers of four refractory oxide materials, Al_2O_3, $Cr:Al_2O_3$, $Nd:YAG$, and $LiNbO_3$. These materials exhibit similar growth characteristics and yield fibers of comparable quality. Fibers as small as $20 \mu m$ in diameter and as long as 20 cm have been grown. Measured optical losses at $1.06 \mu m$ for a 10-cm-long, 170-μm-diam $Cr:Al_2O_3$ fiber were 0.074 dB/cm.

INTRODUCTION

The unique combination of material properties and geometry found in single-crystal optical fibers offers intriguing capabilities in a variety of optical devices. Three refractory oxide materials typify the broad range of potential applications.

The large nonlinear coefficients of $LiNbO_3$ suggest its use for modulators, signal processors, and parametric sources. Miniature lasers made from Nd:YAG fibers[1] have been known for several years. Such active fibers might also be used as in-line amplifiers in conventional glass fiber systems. Sapphire's high melting point and favorable optical properties make it useful in applications such as high-temperature thermometry.[2]

The optimal growth or preparation technique to achieve fiber devices in a variety of single-crystal materials is not yet clear. The methods thus far proposed fall into four categories: hot rolling,[3] edge defined growth and its variants,[4-6] Bridgman growth in capillary tubing,[7,8] and miniature pedestal growth.[9,10] The first three growth approaches require a crucible or die with materials that are compatible with the crystal growth conditions. In addition, the small diameter capillaries or orifices necessary to define crystal growth boundaries have to be produced with the same diameter tolerances that apply to the finished fiber. In order to avoid these problems we have chosen to pursue the laser heated pedestal growth method[10] first applied to optical fiber growth by Burrus and Stone.[11]

Our prior efforts to produce optical fiber devices using the pedestal growth method have been hampered by poor fiber quality.[12] In particular, diameter fluctuations and resultant surface irregularities have led to unacceptably large optical transmission losses. We believe these diameter fluctuations stem from mechanical and optical irregularities occurring during fiber growth rather than from some fundamental crystal growth instability. We have thus designed and built a crystal growth apparatus to produce optical quality single-crystal fibers. The present paper focuses on the

fiber growth apparatus and reports our initial growth results.

I. REQUIRED FIBER CHARACTERISTICS

The growth of single-crystal fibers is motivated by their application to passive, active, and nonlinear optical devices. The device application determines the required crystal fiber characteristics. Important crystal fiber parameters include length, diameter, and optical attenuation.

Optical loss can stem from a number of causes including bulk crystal imperfections, index of refraction variations, diameter fluctuations, and surface defects. The first two causes of loss are present in conventional crystal growth while the latter two are unique to the fiber geometry. The optical loss induced by surface defects and diameter fluctuations depends strongly on the azimuthal dependence and spatial frequency of the perturbation. We estimate losses on the order of 25% for a 1% random diameter fluctuation in a 5-cm-long, 25-μm-diam fiber.

The optical losses can be reduced by using a diffused cladding if the diffusion depth is large compared to the scale length of the diameter variations. Diffused cladding could be accomplished in different ways; for example, out diffusion of Cr^{+3} ions from ruby fibers[13] or in diffusion of protons in c-axis $LiNbO_3$ fibers.[14]

Most optical crystal fiber devices require fiber lengths less than 5 cm with fiber diameters below 200 μm. Small fiber diameters are particularly important in nonlinear optical devices, since tight beam confinement leads to improved nonlinear conversion efficiency. In some passive device applications, such as high-temperature sapphire thermometry,[2] the acceptable optical losses can be quite large and thus fiber diameter variations of several percent are tolerable. Nonlinear interactions, particularly those involving a fiber within a resonator, are more sensitive to diameter fluctuations. We estimate that for a nondiffused cladding, diameter fluctuations must be in the 0.1%–1% range for a useful nonlinear fiber. We have designed and built a crystal growth

Laser-heated miniature pedestal growth apparatus for single-crystal optical fibers

M. M. Fejer, J. L. Nightingale, G. A. Magel, and R. L. Byer

Applied Physics Department, Edward L. Ginzton Laboratory of Physics, Stanford University, Stanford, California 94305

We have designed and built a single-crystal fiber growth apparatus. The apparatus employs novel optical, mechanical, and electronic control systems that enable the growth of high optical quality single-crystal fibers. We have grown oriented single-crystal fibers of four refractory oxide materials, Al_2O_3, $Cr:Al_2O_3$, $Nd:YAG$, and $LiNbO_3$. These materials exhibit similar growth characteristics and yield fibers of comparable quality. Fibers as small as $20 \mu m$ in diameter and as long as 20 cm have been grown. Measured optical losses at $1.06 \mu m$ for a 10-cm-long, $170-\mu m$-diam $Cr:Al_2O_3$ fiber were 0.074 dB/cm.

INTRODUCTION

The unique combination of material properties and geometry found in single-crystal optical fibers offers intriguing capabilities in a variety of optical devices. Three refractory oxide materials typify the broad range of potential applications.

The large nonlinear coefficients of $LiNbO_3$ suggest its use for modulators, signal processors, and parametric sources. Miniature lasers made from $Nd:YAG$ fibers[1] have been known for several years. Such active fibers might also be used as in-line amplifiers in conventional glass fiber systems. Sapphire's high melting point and favorable optical properties make it useful in applications such as high-temperature thermometry.[2]

The optimal growth or preparation technique to achieve fiber devices in a variety of single-crystal materials is not yet clear. The methods thus far proposed fall into four categories: hot rolling,[3] edge defined growth and its variants,[4–6] Bridgman growth in capillary tubing,[7,8] and miniature pedestal growth.[9,10] The first three growth approaches require a crucible or die with materials that are compatible with the crystal growth conditions. In addition, the small diameter capillaries or orifices necessary to define crystal growth boundaries have to be produced with the same diameter tolerances that apply to the finished fiber. In order to avoid these problems we have chosen to pursue the laser heated pedestal growth method[10] first applied to optical fiber growth by Burrus and Stone.[11]

Our prior efforts to produce optical fiber devices using the pedestal growth method have been hampered by poor fiber quality.[12] In particular, diameter fluctuations and resultant surface irregularities have led to unacceptably large optical transmission losses. We believe these diameter fluctuations stem from mechanical and optical irregularities occurring during fiber growth rather than from some fundamental crystal growth instability. We have thus designed and built a crystal growth apparatus to produce optical quality single-crystal fibers. The present paper focuses on the fiber growth apparatus and reports our initial growth results.

I. REQUIRED FIBER CHARACTERISTICS

The growth of single-crystal fibers is motivated by their application to passive, active, and nonlinear optical devices. The device application determines the required crystal fiber characteristics. Important crystal fiber parameters include length, diameter, and optical attenuation.

Optical loss can stem from a number of causes including bulk crystal imperfections, index of refraction variations, diameter fluctuations, and surface defects. The first two causes of loss are present in conventional crystal growth while the latter two are unique to the fiber geometry. The optical loss induced by surface defects and diameter fluctuations depends strongly on the azimuthal dependence and spatial frequency of the perturbation. We estimate losses on the order of 25% for a 1% random diameter fluctuation in a 5-cm-long, $25-\mu m$-diam fiber.

The optical losses can be reduced by using a diffused cladding if the diffusion depth is large compared to the scale length of the diameter variations. Diffused cladding could be accomplished in different ways; for example, out diffusion of Cr^{+3} ions from ruby fibers[13] or in diffusion of protons in c-axis $LiNbO_3$ fibers.[14]

Most optical crystal fiber devices require fiber lengths less than 5 cm with fiber diameters below $200 \mu m$. Small fiber diameters are particularly important in nonlinear optical devices, since tight beam confinement leads to improved nonlinear conversion efficiency. In some passive device applications, such as high-temperature sapphire thermometry,[2] the acceptable optical losses can be quite large and thus fiber diameter variations of several percent are tolerable. Nonlinear interactions, particularly those involving a fiber within a resonator, are more sensitive to diameter fluctuations. We estimate that for a nondiffused cladding, diameter fluctuations must be in the 0.1%–1% range for a useful nonlinear fiber. We have designed and built a crystal growth
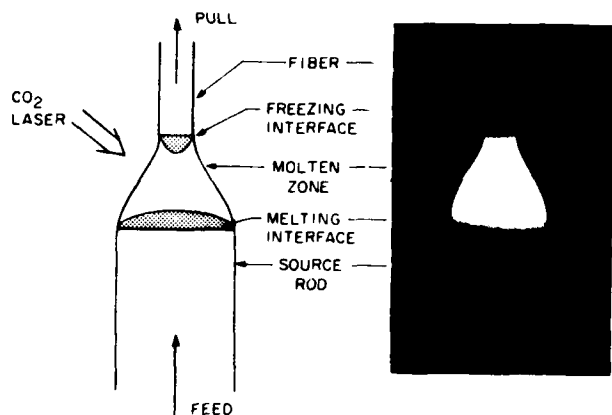
FIG. 1. Schematic diagram and corresponding photomicrograph of fiber growth. The photomicrograph depicts growth of a 190-μm LiNbO$_3$ fiber from a 570-μm-diam source rod. The fiber is supported from above by wetting an oriented seed crystal (not shown). The growth ridges faintly visible on the fiber are discussed later in the text.

apparatus to grow fibers with these length, diameter, and diameter stability characteristics.

II. DESCRIPTION OF GROWTH APPARATUS

A. Design overview

Figure 1 illustrates the miniature pedestal growth of a single-crystal fiber. A tightly focused CO_2 laser, emitting 10.6-μm radiation is the heat source used to melt the refractory material. The source rod may be fabricated from single-crystal,[11] polycrystalline, sintered,[13] or pressed power[15] material. The seed rod defines the crystallographic orientation of the fiber. Growth proceeds by simultaneous upward translation of the seed and source rods with a molten zone positioned between them. The laser focal spot, and consequently the molten zone, remain fixed during fiber growth. The source rod to fiber diameter ratio is set by mass conservation to be the square root of the fiber to source rod translation rate. Typical fiber growth rates range from 1–10 mm/min with diameter reductions of approximately three.

In our system ground rods 500 μm in diameter serve as the initial source for fiber crystal growth. The small rod di-

ameter provides the ability to grow materials with melting points exceeding 2000°C using only a few watts of laser power. An initial growth step reduces the 500-μm-diam rods to a 170-μm-diam fiber. Subsequent diameter reductions using the fiber as a source rod are also possible.

In order to achieve a constant fiber diameter, stable fiber growth conditions must be realized. This in turn dictates smooth source feed and fiber pull rates, stable laser power, and symmetric heat input into the molten zone.

B. Optical system

A block diagram and photograph of the fiber growth apparatus are shown in Figs. 2 and 3, respectively. A 15-W polarized waveguide CO_2 laser (California Laser, model 82-15000-P-W)[16] served as the heat source for crystal growth. The water-cooled laser cavity is temperature stabilized and produces a polarized HE_{11} output mode with power fluctuations less than 1%.

The laser power and beam pointing are most stable if the laser is allowed to run at constant high power. Therefore, an electro-optic power control system is used to vary the laser power incident on the molten zone. The system consists of a ZnSe quarter-wave plate, CdTe electro-optic crystal, and ZnSe polarizer/analyzer. The measured system dynamic range is greater than 100:1. Provisions for modulating the incident laser power have been incorporated into the control circuitry to allow growth of a fiber with controlled diameter variations. Such periodic variations could serve as a distributed Bragg reflector eliminating the need for conventional mirrors in fiber resonator devices.

The CO_2 laser beam (invisible) emerging from the polarizer is combined with a HeNe laser beam (visible) on a dichroic mirror. The visible coincident HeNe beam facilitates CO_2 alignment down the remainder of the optical train. After passing through a ZnSe focusing telescope and some beam steering optics, the CO_2 beam enters the controlled atmosphere growth chamber.

Within the growth chamber a novel optical system focuses the laser beam onto the fiber in a 360° axially symmet-
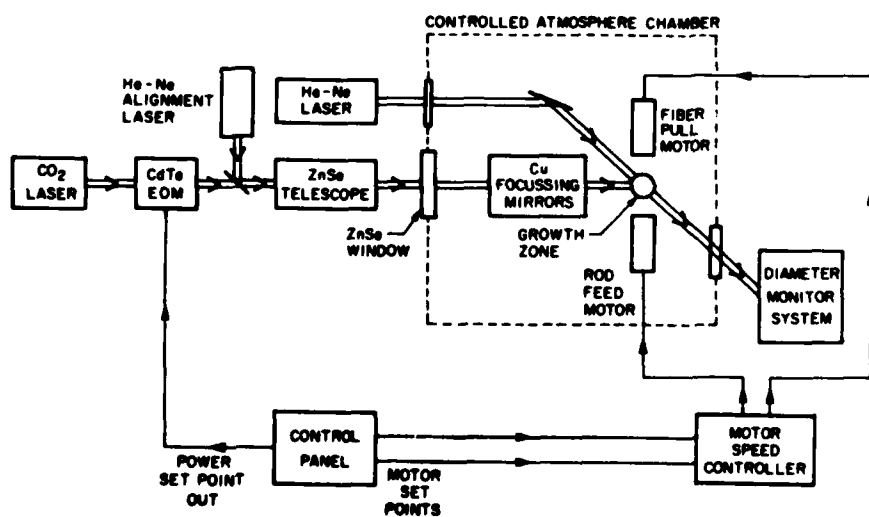

FIG. 2. Block diagram of fiber growth apparatus.

MICROSCOPE

CONTROL PANEL

CO₂ LASER
POWER MONITOR

He - Ne
ALIGNMENT
LASER

- CONTROLLED
  ATMOSPHERE
  CRYSTAL
  GROWTH
  CHAMBER

- FOCUSING
  TELESCOPE

CO₂ LASER

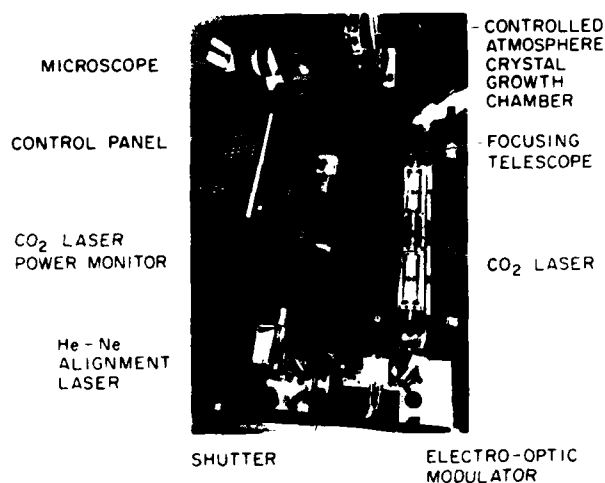SHUTTER   ELECTRO-OPTIC
           MODULATOR

FIG. 3. Photograph of fiber growth apparatus. The diameter measurement system is not installed. A plastic dust cover which normally protects the optical train has been removed for the photograph.

ric distribution as shown in Fig. 4. The symmetric irradiance prevents cold spots in the growth zone and represents a significant improvement over the previously used two-beam,[13] rotating periscope,[17] or ellipsoidal[18] focusing systems. An optical element incorporated into the design is a reflaxicon,[19] which consists of an inner cone surrounded by a larger coaxial cone. In order to achieve good optical performance it is critical that the reflaxicon's two cones be accurately aligned.

A mated surface design, using diamond turned copper optical components, manufactured by Pneumo Precision,[20] assures centering of the two cone axes. A gold coating on the copper optical surfaces enhances reflectivity and protects the copper substrate. The reflaxicon and parabolic mirror provide near diffraction limited $f/2$ focusing, yielding a minimum spot size of 30μm. This tight focus is important for the stable growth of small diameter fibers. The focal spot size can be controlled by modifying the input beam divergence with the focusing telescope. Motorized x–y states on the fiber and source rod translation devices permit adjustment of the fiber position with respect to the fixed laser focal spot.

C. Mechanical system

Previous miniature pedestal growth systems have used lead screw translation. The lead screw fiber translation approach has the drawback that the fiber support point moves away from the melt zone as the fiber grows. The growth zone is thus increasingly sensitive to mechanical perturbations for small diameter and/or long fibers. Moreover, lead screw travel limits the total fiber length.

To alleviate these problems we adopted the belt drive system shown in Fig. 5. The fiber is driven by a polyester cord reinforced urethane belt, which in turn is driven by a dc motor through a speed reducing gearhead. An optical encoder, attached to the dc motor, allows locking the motor speed to a stable reference frequency. A V groove etched in silicon[21] and overcoated with SiO_2 guides the fiber to prevent

UPPER
TRANSLATOR

PARABOLOIDAL
MIRROR

CO₂ LASER
BEAM

TURNING
MIRROR

LOWER
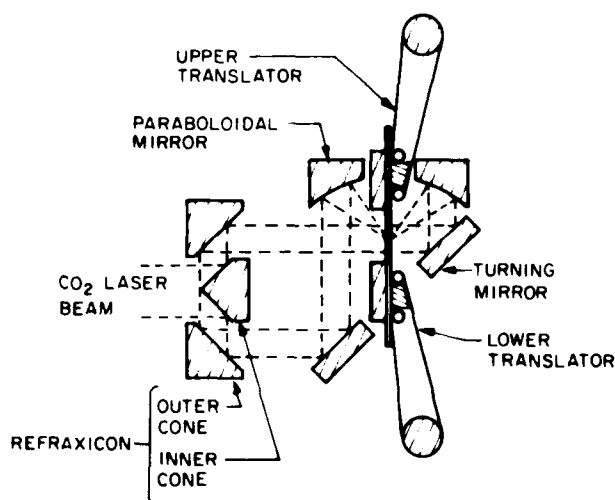TRANSLATOR

OUTER
CONE

REFRAXICON

INNER
CONE

FIG. 4. Photograph of sapphire fiber growth showing optical focusing elements and head of lower translator. A cross-sectional diagram of focusing optics and translators is also shown.

FIBER

1 cm

FIBER

V-BLOCK

FLOATING
BLOCK

IDLER
PULLEYS

BELT

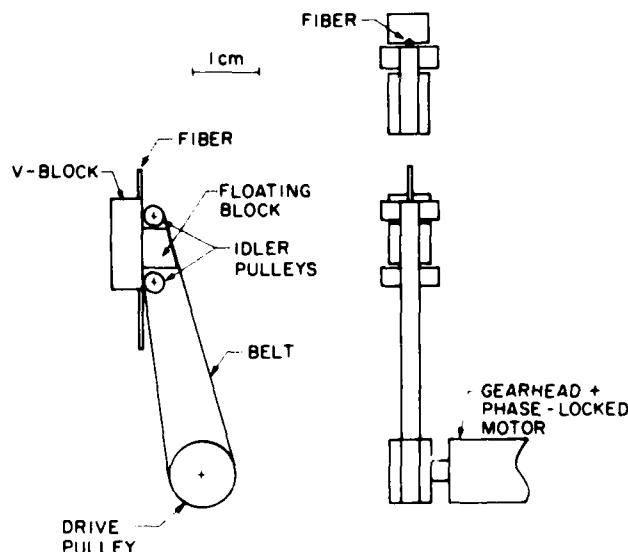GEARHEAD +
PHASE-LOCKED
MOTOR

DRIVE
PULLEY

FIG. 5. Detail of fiber translator.

side-to-side wobble. It provides a smooth, hard sliding surface along the fiber axis.

A phase-locked control circuit enables stable dc motor operation over a 100:1 speed range with acquisition times of 100 ms. A useful control option allows fixing the fiber to source rod speed ratio while adjusting growth speed. Since the fiber diameter has starting transients in the initial phases of growth, a slow growth rate allows time for the operator to make adjustments. As equilibrium conditions are reached growth speed can be conveniently increased without changing the fiber diameter.

The motor control system ensures motor velocity stabilization to frequencies above the mechanical response time of the drive system. Gear noise introduced in the speed reducing gearhead between the dc motor and belt drive pulley is a possible source of fiber translation fluctuation. The magnitude of this noise is not known. However, measurements of the actual fiber translation velocity indicate a jitter of less than 3%, the measurement resolution.

Fiber motion orthogonal to the translation direction is limited only by fiber straightness and diameter uniformity. Uniform diameter source rods are fabricated using a Boccadoro[21] model FB40 centerless grinder. We have ground rods of Al_2O_3, YAG, and $LiNbO_3$ to diameters of 300–600 μm in lengths up to 12 cm, with a taper of less than 1 μm/cm. For these source rods, the measured side-to-side wobble during translation is less than 3 μm, the measurement resolution.

During growth the molten zone is situated 1 cm above the lower translator. The upper translator has two operating positions, 1 and 3.5 cm above the melt. The raised position allows growth of an approximately 3-cm-long fiber without the newly grown fiber contacting the translator. The seed for this growth is typically an oriented crystal mounted in a capillary tube.

Longer fiber lengths are obtained using the lower position of the upper translator and a previously grown 3-cm-long fiber as a seed crystal. In this case both the newly grown fiber and the seed crystal pass through the upper translator. The diameter of the fiber must be matched to that of the seed crystal to within ± 10% to avoid jamming the translator. The small irregularities in fiber diameter resulting from the joint between the seed crystal and new growth can give rise to unacceptably large molten zone side-to-side wobble. This forces the addition of an 8-mm-long glass capillary tube guide mounted onto the end of the upper translator. For growth of a 170-μm-diam fiber a 200-μm-diam guide provides the necessary position stability.

D. Diameter measurement system

Another important feature of the growth apparatus is a high-speed noncontact diameter measurement system. As currently used the system monitors the fiber diameter during growth. A planned improvement in the growth apparatus will be to use the diameter measurement system to provide an error signal in a diameter stabilization feedback loop. In order to grow fibers with 0.1% diameter stability at mm/min growth rates the diameter measurement system must have a measurement rate ≥100 Hz, a diameter resolution

<0.05%, an axial resolution as small as 5 μm, and a working distance ≥ 100 mm to avoid obstruction of the CO_2 focusing system. No commercial system was available which met all these criteria.

We designed and built the fiber diameter system shown schematically in Fig. 6. A helium–neon laser beam illuminates one side of the fiber. The rays passing through the fiber and those reflected off the fiber surface interfere in the far field to form a series of light and dark fringes whose period is inversely proportional to the fiber diameter.[23] By imaging the interference pattern on a photodiode array and electronically tracking one of the fringes as it changes position in response to fiber diameter changes, a voltage proportional to the diameter change is derived. As built, the system has a diameter resolution better than 0.02%, an axial resolution of 5 μm, and a measurement rate of 1 kHz. A detailed description of the diameter measurement system is given by Fejer, Magel, and Byer.[24]

III. RESULTS

Four crystalline materials have been grown to date: sapphire (Al_2O_3), sapphire with 0.05 wt.% chromium (ruby), YAG with 0.9 wt.% neodymium, and lithium niobate ($LiNbO_3$). Growth characteristics of the chromium doped ruby were identical to those of the pure sapphire. Growth orientations for the fibers were ⟨001⟩ for sapphire, ⟨111⟩ for YAG, and both ⟨001⟩ and ⟨100⟩ for lithium niobate. Fibers as small as 20 μm in diameter and as long as 20 cm have been grown (see Table I). Fiber growth speeds ranged from 0.3 to 30 mm/min.

Typical diameter reductions are approximately three to one. Larger diameter reductions result in less stable growth and yield fibers with larger diameter fluctuations. Smaller diameter reductions yield good quality fibers but require more steps to reach the desired diameter. The observed correlation between diameter reduction and growth stability agrees qualitatively with the theoretical analysis of Surek and Coriell.[25]

Even though the melting temperatures range from 2045° to 1260 °C for these materials, their fiber growth characteristics are similar. Molten zone length is determined by the incident laser power. For optimum growth stability the laser power was adjusted to yield the molten zone shape depicted in Fig. 7. For all materials investigated the optimal molten zone shape is similar, with a height–width ratio of
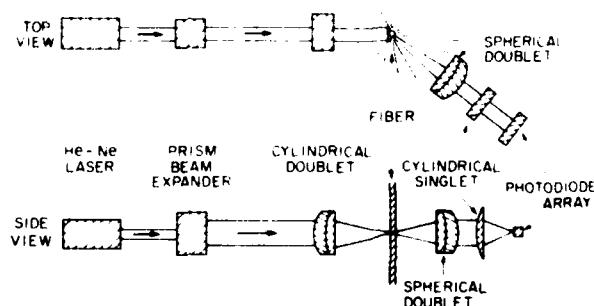

FIG. 6. Schematic diagram of fiber diameter measurement system.

TABLE I. Length, diameter, and crystallographic orientation for some single-crystal fibers grown with the apparatus.

Material	Orientation	Length (cm)	Diameter (μm)
Al₂O₃	(001)	20	170
		3.0	50
Al₂O₃ + 0.05 wt.% Cr	(001)	10.0	170
		3.0	20
YAG + 0.9 wt.% Nd	(111)	3.0	110
		3.0	40
LiNbO₃	(001)	3.0	50
	(100)	3.0	170

(a)

(b)

(c)

|——————————| 100 μ

FIG. 8. Scanning electron micrographs of LiNbO₃ fibers: (a) cleaved cross section of a-axis fiber, (b) cross section of c-axis fiber, (c) surface of c-axis fiber. The internal concentric ring pattern and dark central area in (b) are artifacts of the procedure used to obtain the cross section. In (c) note the sharply defined growth ridges at the right boundary and near the left edge.

0.9 ± 0.15 for a 3 to 1 diameter reduction. Typical power levels necessary to grow from 500-μm Al₂O₃ or LiNbO₃ rods are 4.8 and 1.5 W, respectively.

In Fig. 7 the growing fiber is invisible since its smooth sides scatter much less light than those of the ground source rod. The solid–liquid growth interface is evident as the slightly darker bowl-shaped region ᴀᴛ the top of the molten zone. The curvature of this isothermal surface reflects the radial temperature gradients present. The measured angle between the growing fiber and the molten zone at the periphery (meniscus angle) is 12° and 8° (± 2°) for sapphire and YAG, respectively. This angle is a material constant independent of fiber growth speed or diameter. Our measured meniscus angle for sapphire (12° ± 2°) is slightly below but not inconsistent with the 17° ± 4° value previously measured by Dreeben, Kim, and Schujko.[28]

A well-defined meniscus angle could not be measured in lithium niobate due to the highly anisotropic fiber cross section. A-axis lithium niobate fibers shows a rectangular cross section with two protruding ridges, while c-axis lithium niobate has three sharply defined growth ridges. These ridges are clearly shown in Figs. 8(a) and 8(b). The ridges run smoothly and continuously down the length of the fiber as shown in Fig. 8(c). The growth ridges found in LiNbO₃ are not evident in either sapphire or YAG fibers, both of which show a slightly rounded hexagonal cross section.

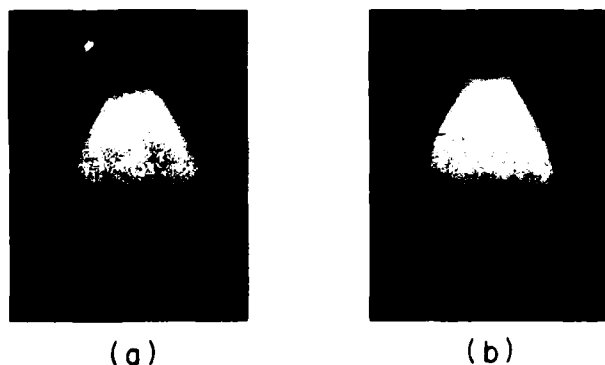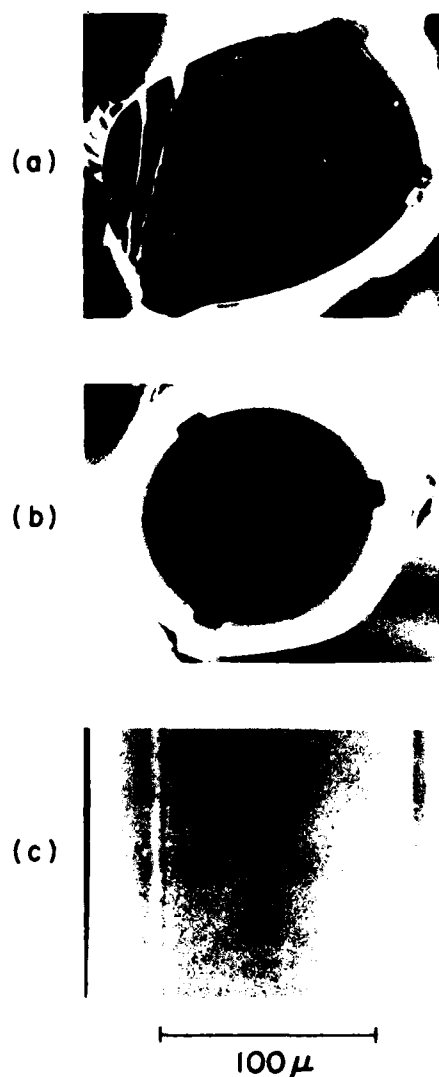Another feature evident in Fig. 8(c) is the excellent fiber

(a)

(b)

FIG. 7. Both photomicrographs illustrate a 3 to 1 diameter reduction from a 500-μm-diam source rod. Materials are (a) Al₂O₃, melting point 2045 °C and (b) Nd:YAG, melting point 1970 °C. Notice the similarity to Fig. 1 showing LiNbO₃, melting point 1260 °C.

diameter control and surface quality. No fiber irregularities exist on the micron scale lengths visible in the figure. On a longer scale length we have demonstrated a rms diameter variation of 1% over a 1 cm length of fiber.

Typical variations in fiber diameter are shown in Fig. 9. This 55-μm-diam ruby fiber was grown at 4.5 mm/min from a 165-μm-diam source rod. The previously described diameter measurement apparatus was used to measure the deviations about the mean diameter. The rms diameter variation over the entire fiber length is 1.7%. The last centimeter of fiber shows a 1% rms diameter variation.

To date all growth has been performed with the growth chamber open to the atmosphere. The as-grown LiNbO₃ fibers have a brownish cast resulting from oxygen loss during growth. Annealing the fiber at 1000 °C in an oxygen atmosphere for several hours recovers a water-white crystal color.

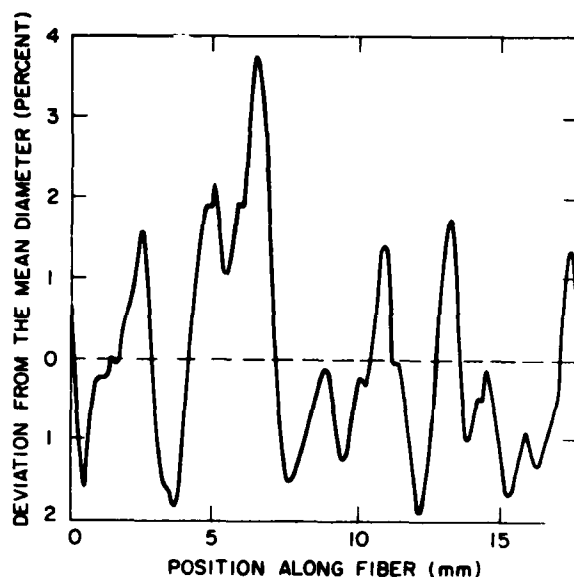A 10-cm-long, 170-μm-diam ruby fiber grown at 3.0 mm/min showed 72% transmission of an incident 1.06-μm

FIG. 9. Diameter variations in a 55-μm-diam ruby fiber measured with the noncontact diameter measurement system.

Nd:YAG laser beam. Taking into account the Fresnel reflection losses from the fiber end faces, the fiber optical loss can be calculated as 1.7%/cm or equivalently, 0.074 dB/cm. In this test no optical cladding was used, the guiding dielectric interface being the ruby fiber surface and the surrounding air.

IV. DISCUSSION

The single-crystal fiber growth apparatus has proven very reliable and easy to use. Over the past year six different operators have grown a total of more than 350 fibers. As many as 14 fibers have been grown on a single day. The time necessary to change from growing one material to another is small, approximately 30 min.

The novel design of the apparatus has allowed the growth of single-crystal fibers with a diameter stability of 1% per centimeter of length. The growth morphology of the crystal fibers is similar to that seen in bulk Czochralski crystal growth. The noncircular nature of the fiber cross section does not introduce additional optical loss since the cross section is invariant with length.

In our initial efforts to propagate light down these fibers we have measured optical losses of < 2% per cm over distances of several centimeters. Losses of this level are acceptable in some device applications such as sapphire fiber thermometry. Efficient active and nonlinear devices demand somewhat lower optical losses. We have designed and constructed a single-crystal fiber growth apparatus based on a laser heated miniature pedestal growth technique. Oriented single-crystal fibers have been grown with diameters of 500

to 20 μm. Planned improvements in fiber diameter control and fiber cladding techniques should allow realization of single-crystal fiber-optical devices.

[1]J. Stone and C. A. Burrus, Fiber Integrated Opt. 2, 19 (1979).

[2]R. R. Dils, J. Appl. Phys. 54, 1198 (1983).

[3]J. A. Harrington, Proc. SPIE 227, 85 (1980).

[4]J. T. Bridges, J. S. Hasiak, and A. R. Strand, Opt. Lett. 5, 85 (1980).

[5]H. E. La Belle, Jr. and A. I. Mlavsky, Mater. Res. Bull. 6, 571 (1971).

[6]B. Chalmers, H. E. La Belle, Jr., and A. I. Mlavsky, Mater. Res. Bull. 6, 681 (1971).

[7]J. L. Stevenson and R. B. Dyott, Electron. Lett. 10, 449 (1974).

[8]H. P. Weber, P. F. Liao, B. C. Tofield, and P. M. Bridenbaugh, Appl. Phys. Lett. 26, 692 (1975).

[9]D. B. Gasson and B. Codkayne, J. Mater. Sci. 5, 100 (1970).

[10]J. S. Haggerty, NASA Report No. Cr-120948, 1972.

[11]C. A. Burrus and J. Stone, Appl. Phys. Lett. 26, 318 (1975).

[12]M. Fejer, R. L. Byer, R. Feigelson, and W. Kway, Proceedings of the SPIE Advances in Infrared Fibers II (1982), p. 320.

[13]C. A. Burrus and L. A. Coldren, Appl. Phys. Lett. 31, 383 (1977).

[14]J. L. Jackel, C. E. Rice, and J. J. Vaselka, Jr., Appl. Phys. Lett. 41, 607 (1982).

[15]J. Stone and C. A. Burrus, J. Appl. Phys. 49, 2281 (1978).

[16]California Laser Corporation, 1070 Commerce Street, San Marcos, CA 92069.

[17]J. E. Midwinter, Optical Fibers for Transmission (Wiley, New York, 1979), p. 194.

[18]U. C. Paek, Appl. Opt. 13, 1383 (1974).

[19]W. R. Edmonds, Appl. Opt. 12, 1940 (1973).

[20]Pneumo Precision Incorporated, Precision Park, Keene, NH 03431.

[21]F. Boccadoro, Via Dr. Varesi, CH-6600 Locarno, Switzerland.

[22]C. M. Schroeder, BSTJ 57, 91 (1978).

[23]D. H. Smithgall, L. S. Watkins, and R. E. Frazee, Jr., Appl. Opt. 16, 2395 (1977).

[24]M. M. Fejer, G. A. Magel, and R. L. Byer (to be published).

[25]T. Surek and S. R. Coriell, J. Cryst. Growth 37, 253 (1977).

[26]W. Bardsley, F. C. Frank, G. W. Green, and D. T. J. Hurle, J. Cryst. Growth 23, 341 (1974).

[27]T. Surek, J. Appl. Phys. 47, 4384 (1976).

[28]A. B. Dreeben, K. M. Kim, and A. Schujko, J. Cryst. Growth 50, 126 (1980).

1. D. J. Williams, Ed., "Nonlinear Optical Properties of Organic and Polymeric Materials," *ACS Symposium Series 233* (1983).
2. B. F. Levine, Chem. Phys. Lett 32, 516 (1926); J. L. Oudar and D. S. Chemla, J. Chem. Phys. 66, 2664 (1977).
3. S. Tomaru, S. Zombutsu, M. Kawachi, and M. Kobayashi, J. Chem. Soc. Chem. Commun. 1207 (1984).

THM45   Proton-exchanged waveguides in MgO: LiNbO₃

M. DIGONNET, Litton Systems, Inc., Chatsworth, Calif. 91311; M. M. FEJER and ROBERT L. BYER, Stanford U., Ginzton Laboratory, Stanford, Calif. 94305.

It has recently been shown that LiNbO₃ doped with 5% MgO (MgO:LiNbO₃) has a substantially reduced photorefractive response compared with undoped LiNbO₃.[1] This material is thus very promising for improving the efficiency of linear and nonlinear guided wave devices which have previously been affected by photorefractive-index damage. We have studied the proton-exchange process in MgO:LiNbO₃ and undoped congruent LiNbO₃ and compared our results for the two materials. Results were similar, with the most significant differences being increased resistance of the y face to etching and lower diffusion coefficients in the doped material.

Waveguides were fabricated in x- and y-cut 5% MgO-doped LiNbO₃ grown by Crystal Technology of Palo Alto, Calif., and compared with guides made in congruent LiNbO₃ from the same manufacturer. Proton exchanges took place in melts of benzoic acid containing various concentrations of lithium benzoate.[2] The lithium benzoate provides a means for controlling the proton concentration in the exchanged region.

The index profiles were obtained from measured prism launching angles by means of a standard inverse WKB method. Figure 1 shows a typical set of index profiles for several wavelengths in an x-cut MgO:LiNbO₃ waveguide. The essentially step nature of the index profile is the same as seen in undoped waveguides. The ordinary index profile, obtained from the dependence of the propagation constants on direction of propagation, is also shown.

The depth of the waveguides depended on the square root of the exchange time indicating a diffusionlike behavior. The diffusion coefficient D, defined by $D = \sqrt{4dt}$, where d is the depth of the guide and t is the exchange time, is shown in Fig. 2. The diffusion coefficient is seen to be 50–60% slower in doped material than undoped.

Waveguides fabricated in doped y-cut samples showed no evidence of etching after 4 h of exchange in pure benzoic acid, while undoped y-cut samples showed significant etching in much shorter times. Diffusion rates were found to be essentially the same for x- and y-cut MgO·LiNbO₃.

Figure 3 shows the dispersion of Δn_e for two different Li concentrations in the melt and a single-pole Sellmeier fit to the data. The index change was found to vary substantially with wavelength, from ~0.18 at 458 nm to 0.12 at 820 nm. For a given Li concentration, the index change was found to be 0.002–0.003 larger at 633 nm in doped x-cut material compared with undoped.

Preliminary results indicate an approximately twofold increase in resistance to photorefractive damage in the doped guides. More detailed studies of the damage resistance of these guides will be reported.   **(Poster paper)**

---

1. Z. Gi-Guo et al., in *Proceedings, Eleventh International Quantum Electronics Conference*, IEEE Catalog No. 80, CH1561-0 (June 1980), p. 631; D. A. Bryan et al., Appl. Phys. Lett. 44, 847 (1984).
2. J. Jackel et al., J. Appl. Phys. 55, 269 (1984).

THM46   Faraday rotator for UV lasers and its impact on KrF laser technology

K. UEDA, H. NISHIOKA, H. HISANO, and H. TAKUMA, UEC Institute for Laser Science, Chofushi, Tokyo 182, Japan.

In a laser system composed of a master oscillator and a chain of amplifiers, the isolation of each stage is essential. Faraday rotators are used in most of the modern glass laser systems of large scale to eliminate buildup of a backward propagating beam.

CO₂ lasers oscillate in the wavelength range where there is a great deal of difficulty in finding an appropriate material for a Faraday rotator. Thus other means, such as saturable absorbers or plasma switches, are used as isolators. In excimer lasers which operate in the UV range, interstage coupling has been eliminated by separating each stage just far enough from adjacent ones.

None of these conventional isolation methods is competitive with a Faraday isolator in isolation, efficiency, and convenience, and the introduction of a Faraday rotator should greatly improve the stability and design flexibility of excimer lasers. In spite of this, a Faraday rotator for UV lasers has not been developed, probably because of the feeling that it may be difficult to find appropriate material for UV Faraday rotators. However, the Verdet constants of common transparent materials, such as water and synthetic quartz, increase approximately in proportion to the square of the frequency and take at 248 nm even larger values than that of Faraday rotator glass for 1.06-μm Nd:glass lasers.

We have demonstrated for the first time that 90° of Faraday rotation can be obtained for 248-nm output of a KrF laser using a 5-cm long quartz optical cell filled with water in ~10 kOe of an axial magnetic field as shown in Fig. 1. The water is highly transparent in the ultraviolet, and the present result demonstrates that a UV Faraday isolator can be constructed easily since we know that polarizers with sufficient extinction ratio are available for KrF lasers.

By the application of Faraday isolators significant improvements in the performance of KrF laser systems can be achieved, and some advanced designs may be possible. We propose a new scheme of a long-pulse amplifier in which several short pulses, each of which is traveling in one of several unidirectional ring resonators, are alternately amplified, as shown in Fig. 2. The input and output of each optical pulse are controlled by switching the polarization plane with a Pockels cell. We have analyzed such a system and find that it may be a simple and economical means of pulse compression. This preliminary experiment shows that such a system is feasible.   **(Poster paper)**

THM47   Band-to-band Auger processes in 1.55-μm InGaAsP semiconductor lasers

W. BARDYSZEWSKI, U. Warsaw, Institute of Theoretical Physics, Hoza 69, 00 681 Warsaw, Poland, and D. YEVICK, U. Lund, Department of Theoretical Physics, Solvegatan 14a, S-223 62 Lund, Sweden.

Although Auger processes have for several years been cited to explain the temperature sensitivity of long-wavelength InGaAsP lasers, many previous theoretical calculations of the Auger coefficients have yielded values which are about an order of magnitude larger than those currently measured

---

using, e.g., picosecond pulse techniques.[1] Since several recent publications have noted that much of this discrepancy may be attributed to the use of incorrect k·p wave functions,[2,3] we have recently evaluated the Auger coefficients of p-GaAs, 1.3-μm InGaAsP, and 1.3-μm AlGaInAs in a manner fully consistent with the four-band Kane model. In contrast to previous treatments, we also applied the correct first-order electron self-energy to evaluate the effects of phonon-assisted Auger processes.[4] To avoid further approximations to the proper energy-momentum dispersion relation, wave function overlap integrals, and Fermi factors, we employ a Monte Carlo integration procedure in conjunction with an analysis of the phase-space restrictions imposed by the threshold condition and Fermi factors. While our results for the Auger coefficients of both p-GaAs and In₀.₇₀Ga₀.₃₀As₀.₆₄P₀.₃₆ are in good agreement with experiment, the accuracy of our method is severely limited by uncertainties in the band structure parameters.

Turning to our new theoretical results for 1.55-μm undoped In₀.₅₈Ga₀.₄₂As₀.₉₀P₀.₁₀, our calculated values for the temperature variation of the pure collision and the total (phonon-assisted and pure collision) Auger coefficients at an excess carrier concentration of 2.0×10^{18} cm⁻³ are given, respectively, by the dotted and solid lines of Fig. 1(a) (CHCC coefficients) and Fig. 1(b) (CHSH coefficients). As the contribution of CHSH phonon-assisted processes are negligible, only one line is present in the latter figure. Note also that CHSH processes give the dominant contribution to the total Auger coefficient except at the endpoints of the graphs. The primary band structure parameters input to this calculation are split-off band separation, $\Delta = 0.32$ eV, conduction electron mass, $m_c = 0.045 m_e$, heavy hole mass, $m_h = 0.44 m_e$, split-off band mass, $m_s = 0.12 m_e$, and light-hole mass, $m_1 = 0.057 m_e$. The phonon coupling parameters are obtained by interpolation from measured binary values. In considering these results, it should be noted that the band-structure parameters given above are those employed by Dutta and Nelson in all except their latest publication, which unfortunately only considers the composition In₀.₇₀Ga₀.₃₀As₀.₆₄P₀.₃₆.[5] We have noted previously that use of these revised parameters decreases the total 1.3-μm InGaAsP Auger coefficient by ~50%. The CHCC Auger coefficient is further particularly sensitive to details of the band structure, and the four-band Kane model may in this case be inadequate given the high momentum values attained by the Auger electron. Our research was funded by STU and NFR, Sweden.
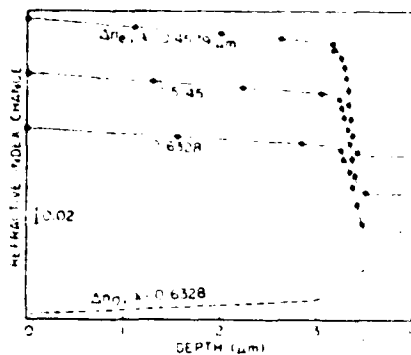
    (Poster paper)

1. B. Sermage, H. J. Eichler, J. P. Heritage, R. J. Nelson, and N. K. Dutta, Appl. Phys. Lett. 42, 259 (1983).
2. B. L. Gelmont, Z. N. Sokolova, and V. B. Khalfin, Sov. Phys. Semicond. 17, 280 (1983).
3. M. G. Burt and C. Smith, J. Phys. C 17, L47 (1984).
4. G. D. Mahan, *Many Body Physics* (Plenum, New York, 1981), p. 560.
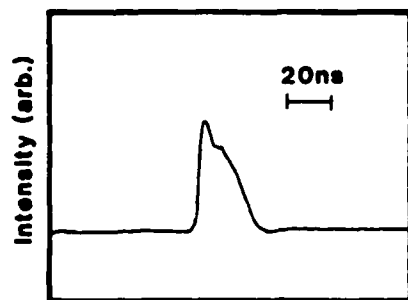5. R. J. Nelson and N. K. Dutta, J. Appl. Phys. 54, 2923 (1983).

THM48   Perfectly contactless scanning of photoactive materials by laser-induced microwave absorption

G. BECK and M. KUNST, Hahn-Meitner-Institut für Kernforschung Berlin, Bereich Strahlenchemie, D-1000 Berlin 39, F. R. Germany.
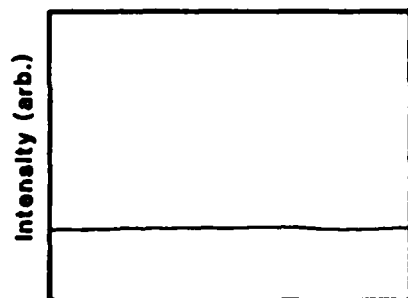
Laser scanning techniques, as applied widely in recent years to resolve local inhomogeneities and to study defects in semiconductor devices and ma-

THM45 Fig. 1. Typical Δn_e and Δn_o profiles in an x-cut MgO:LiNbO$_3$ waveguide exchanged for 3 h in pure benzoic acid.
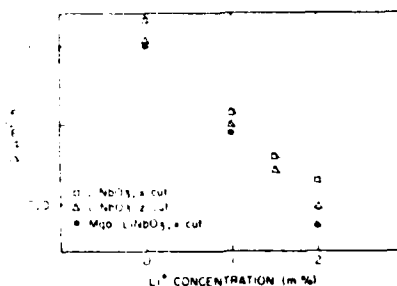
THM45 Fig. 2. Proton diffusion rate in doped and undoped x-cut LiNbO$_3$ as a function of Li concentration in the melt.

THM45 Fig. 3. Δn_e dispersion of x-cut MgO:LiNbO$_3$ for two Li concentrations in the melt.
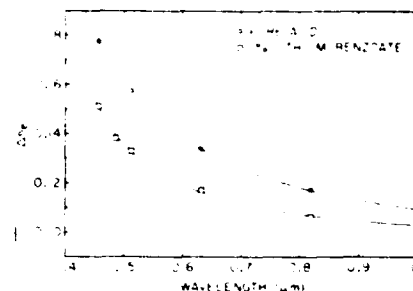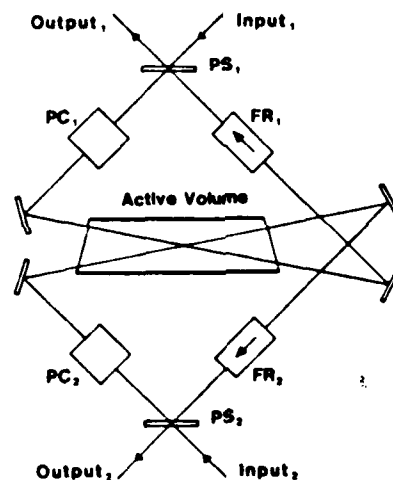
20ns

(a)

(b)

THM46 Fig. 1. Extinction of a KrF laser beam by 90° polarization rotation of a linearly polarized beam in a Faraday rotator using a 5-cm quartz cell filled with water: (a) transmittance of the laser pulse through the cell without a magnetic field and (b) its extinction by the application of the 90° field (~10 kOe).
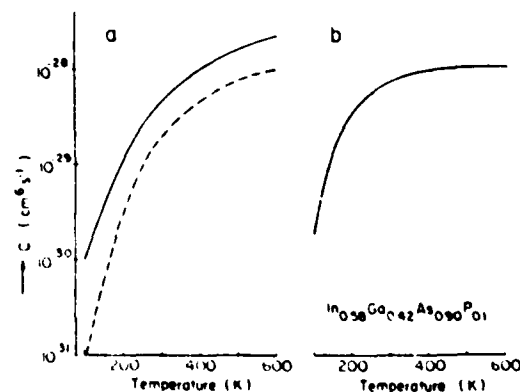
Output,   Input,

PS,

PC,   FR,

Active Volume

PC,   FR,

PS,

Output,   Input,

THM46 Fig. 2. Schematics of the proposed multiring amplifier of short pulses using Faraday unidirectional components: PC, Pockels cell; FR, Faraday rotator; PS, polarization selector.

THM47 Fig. 1. (a) CHCC Auger coefficients and (b) CHSH Auger coefficients for In$_{0.58}$Ga$_{0.42}$As$_{0.90}$P$_{0.10}$ vs temperature. The dashed lines are the contribution of pure collision processes, while the solid lines are the full (pure and phonon-assisted) Auger coefficients. The assumed excess carrier concentration is 2.0×10^{18} cm^{-1}.

width, and antiguiding on the radiation patterns will be discussed. **(Poster paper)**

1. D. R. Scifres, W. Streifer, and R. D. Burnham, IEEE J. Quantum Electron. QE-15, 917 (1979).
2. C. P. Lindsey et al. in Postdeadline Papers, Conference on Lasers and Electro-Optics (Optical Society of America, Washington, D.C., 1984), paper ThR1.
3. J. W. M. Biesterbos et al., IEEE J. Quantum Electron. QE-19, 961 (1983).
4. T. L. Paoli, W. Streifer, and R. D. Burnham, Appl. Phys. Lett. 45, 217 (1984).
5. E. Kapon et al., Appl. Phys. Lett. 44, 389 (1984).

WM34 Laser resonators with nonuniform gain

MARTIN E. SMITHERS, U.S. Army Missile Laboratory, 1538 Four Mile Post Rd., Huntsville, Ala. 35802.

The geometrical optics theory of unstable resonators has recently been broadened to include nonuniform magnification.[1] An important possible application of such resonators is for lasers with nonuniform gain profiles. Here a simple saturable gain model is used to analyze the effect of nonuniform gain profiles on the geometric modes of unstable resonators including those with nonuniform magnification. Thus a comparison of the predicted performance of both uniform and nonuniform magnification resonators is made, such comparison serving as a guide in selecting the most advantageous resonator design for a given gain profile.

In the general case, the resonator magnification $M(r)$ is a function of the transverse coordinate r in the output plane. As found previously,[1] the magnification function $M(r)$ determines the output intensity $I(r)$ in the bare-cavity case. To treat the effect of gain, a single gain sheet located in the output plane is assumed. In the steady state, conservation of energy after a round trip through the resonator yields the condition

$$\Gamma e^{a_0 I(r) I(r) r dr} = I[rM(r)] rM(r) d[rM(r)] \qquad (1)$$

in the axisymmetric case. Here Γ is the linear round-trip loss, and $G(r)$ is the saturated gain. In the case of uniform unsaturated gain G_0 and magnification, Eq. (1) has the usual solution of uniform intensity. However, for nonuniform $G_0(r)$, a uniform intensity solution may also be obtained by requiring the magnification to be a function of r specified by the equation

$$[rM(r)]^2 = 2\Gamma \int_0^r r e^{a_0 r} r dr. \qquad (2)$$

This relation [Eq. (2)] is readily integrated in the case of $G_0(r)$ which is a quadratic (or linear) function of r. This, if it is considered desirable to maintain a uniform intensity profile, may be accomplished even in the case of a nonuniform gain profile by the suitable choice of magnification function.

A general approach to solving Eq. (1) for the intensity is carried out for several example cases. First, the case of a quadratic gain function is treated, and the intensity profile for uniform magnification is calculated. This is compared with the nonuniform magnification case for uniform intensity calculated from Eq. (2). The result is that, for quadratically increasing gain, the intensity also rises quadratically, while for quadratically decreasing gain the intensity decreased very slowly over the range considered. For uniform intensity, the magnification function increases with increasing gain and decreases with decreasing gain, as might be expected. As a final case, a uniform gain profile is considered but with a linearly increasing magnification function. The resulting intensity profile falls off exponentially with

increasing distance. From the plots of intensity, the output power for given size output aperture is estimated and compared for different magnification functions. **(Poster paper)**

1. T. R. Ferguson and M. E. Smithers, J. Opt. Soc. Am. A 1, 653 (1984).

WM35 Numerical optimization study of a self-filtering unstable resonator for high-power, solid-state, and gas lasers

P. G. GOBBI, U. Pavia, Dipartimento di Elettronica, Sezione di Fisica Applicata, 27100 Pavia, Italy; and G. C. REALI, North Texas State U., Physics Department, Center for Applied Quantum Electronics, Denton, Tex. 76203.

A self-filtering unstable resonator (SFUR) is a negative-branch confocal unstable resonator in which the field-limiting aperture, set at the common focal plane of the mirrors, acts as a filter to shape a very smooth spatial beam profile and to cool the hot focal point inside the cavity down to nondamage limits. In Refs. 1 and 2 we demonstrated both theoretically and experimentally that this kind of resonator is highly effective in producing large-volume smooth-profiled beams with an increase in oscillator efficiency and excellent energy transport and focusability.

We report the results of a numerical optimization study carried out to exploit the conditions for the best SFUR operation. We show the results of the eigenvalues and eigenmodes computations. One main result is the extreme high selectivity operated by the intracavity filter which rules out the possibility of multiple-transverse-mode operation $[(\gamma_0/\gamma_1)^2 > 100]$. Furthermore, among the class of $(N_{eq} = \infty)$ resonators we find that the SFUR has the lowest losses with feedback intensity almost twice as high as the geometrical predicted value of $1/M^2$.

An interesting feature of the eigenvalues is their oscillatory behavior when plotted vs the aperture size, and we uncovered that, in the $(N_{eq} = \infty)$ condition, this behavior is regulated by the reduced Fresnel number N_1 relative to the shorter focal length mirror of the cavity.

It is interesting to study in which conditions of mismatched aperture size and positioning the beam quality remains good with an almost Gaussian-shaped profile. We found that a variation of the aperture size of ±10% or a displacement of ±20% its distance from the shorter focal length mirror produces no appreciable change of the mode structure. This has also been verified experimentally.

Also reported is the study of the rate of convergence to the steady state of the cavity modes and the results of the simulations of the beam propagation in different conditions of cavity loading and output beam extraction. **(Poster paper)**

1. P. G. Gobbi and G. C. Reali, "A Novel Unstable Resonator Configuration with a Self-Filtering Aperture," to appear in Opt. Commun.
2. P. G. Gobbi, S. Morosi, G. C. Reali, and A. S. Zarkasi, "Novel Unstable Resonator Configuration with a Self-Filtering Aperture: Experimental Characterization of the Nd:YAG Loaded Cavity," Appl. Opt. 24, 26 (1985).

WM36 Monolithic resonator single crystal fiber laser

J. L. NIGHTINGALE and ROBERT L. BYER, Stanford U., Applied Physics Department, Stanford, Calif. 94305.

We report the first monolithic resonator crystal fiber optical device, a liquid nitrogen-cooled ruby fiber laser. The laser resonator structure is simply formed by the fiber waveguide and the polished fiber

endfaces. The fiber oscillator was 15 mm long with a mean diameter of 60 μm. The lowest-order optical mode for such a fiber has a beam waist approximately one-third the fiber diameter or 20 μm, implying a Rayleigh length in ruby of 3.2 mm. The 15-mm long fiber laser is thus approximately five Rayleigh lengths long and may be considered a guided wave device. In these fibers the waveguiding interface is the ruby liquid nitrogen boundary at the fiber periphery. The large refractive-index difference between these materials coupled with fiber diameter variations of ~2% leads to substantial waveguide losses. The high gain of 77 K ruby allows laser operation despite these losses.

The ruby fiber used was grown by the miniature pedestal growth technique[1,2] using an apparatus developed in our laboratory.[3] The fiber endfaces were fabricated by mounting the fibers in a slotted sapphire block. Unfortunately, the very light fiber (~0.1 mg) had a tendency to bend and wander within the slot. This led to the endfaces being skewed with respect to the fiber axis as well as a loss of endface parallelism. After removal from the polishing fixture an optically thick reflective aluminum coating was vapor deposited on one fiber endface. A photograph of a polished fiber endface is shown in Fig. 1(a). Figure 1(b) shows the fiber mounted in the aluminum holder which supports the fiber during laser tests.

The overall system for ruby laser operation is shown in Fig. 2. We found that laser oscillation could be obtained even with the aluminum mirror removed from the rear fiber endface. The difference in the laser thresholds for the uncoated and aluminum-coated rear endface allows us to estimate the resonator losses. The results indicate a lossy cavity with a round-trip loss of 98.5%. The loss stems about equally from waveguide imperfections and endface misalignment.

The cw laser output was quasi-steady state with power variations of only ±10%. A maximum laser output power of 2.0 mW was observed with 750 mW of 514.5-nm pump radiation. No large-scale spiking was seen due to the high cavity losses and highly multimode transverse beam profile. The laser beam divergence was approximately ten times the diffraction limit.
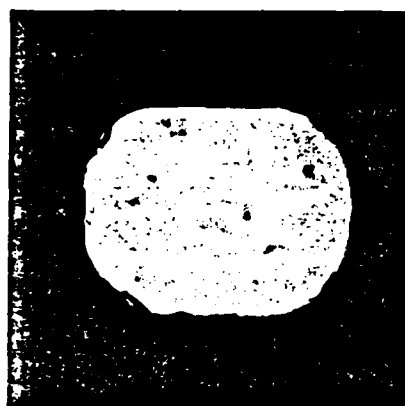
The experience gained in this initial device demonstration will be used to develop a monolithic resonator guided wave Nd:YAG laser system. Progress in this area will be reported. **(Poster paper)**

1. C. A. Burrus and J. Stone, J. Appl. Phys. 49, 3118 (1978).
2. J. Stone and C. A. Burrus, Fiber Integrated Opt. 2, 19 (1979).
3. M. M. Fejer, J. L. Nightingale, G. M. Magel, and R. L. Byer, to be published in Rev. Sci. Instrum. (Nov. 1984).

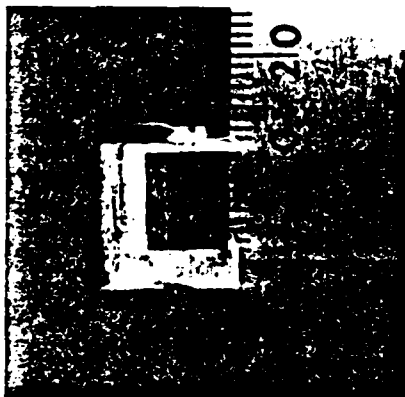### WM37 Amplified spontaneous emission and parasitic oscillations in slab lasers

DAVID C. BROWN, General Electric Research & Development Center, Schenectady, N.Y. 12301; and KOTIK K. LEE, General Electric Co., Armament and Electronic Systems Division, Binghamton, N.Y. 13902.

Recently[1] we reported experimental evidence of the deleterious effect of amplified spontaneous emission on the performance of a highly doped Nd glass slab laser. It was shown that the approximate gain-length product value of ~1.85 should not be exceeded if good laser efficiency is desired. While this rule is generally applicable to unloaded lasers it was nevertheless found to be applicable even in normal mode operation. We have investigated this question by calculating the ratio γ of straight-across (surface) gain in a slab laser to that
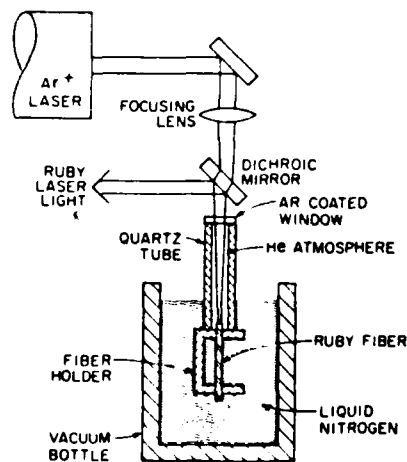
—50 μm—

(a)

(b)

WM36 Fig. 1. (a) Cross section of a polished (1100) axis ruby fiber typical of those used in the laser tests. The minor axis corresponds to the (0001) direction. (b) Single crystal ruby fiber mounted in its fiber holder. The holder supports the fiber during laser tests.

WM36 Fig. 2. Experimental setup used in the cw monolithic resonator ruby fiber laser tests. The fiber is end pumped using focused 514.5-nm radiation from an Ar-ion laser.

THH2 Controlled growth of single-crystal optical fibers

G. A. MAGEL, M. M. FEJER, J. L. NIGHTINGALE, and ROBERT L. BYER, Stanford U., Applied Physics Department, Stanford, Calif. 94305.

The growth of single-crystal optical fibers offers the opportunity to make linear and nonlinear optical devices which are not possible in glass. For example, sapphire fibers could be used in hostile environments where glass could not survive, and waveguide nonlinear and electrooptic devices could be made which may couple better to glass fibers than slab waveguide-integrated optics devices.

We have designed and built a machine for growing fibers of a variety of refractory oxide materials.[1] The technique, called laser-heated miniature pedestal growth,[2] is illustrated in Fig. 1. In this crucibleless method, a CO_2 laser melts the end of a rod of feed material. A seed crystal is dipped into the molten zone thus formed, and the fiber is grown by pulling the seed crystal away from the melt while fresh feed material is simultaneously fed into the molten zone. We have grown more than 400 fibers of Nd:YAG, Al_2O_3 (undoped and doped with Cr or Ti), and $LiNbO_3$ (undoped and Mg doped) in several crystal orientations and with diameters as small as 20 μm. For most device applications, typical fiber lengths are <5 cm, although it is possible to grow longer lengths with our apparatus.

To be useful for devices, the fibers must have a stable diameter to minimize scattering losses. We have built a 16-cm working distance fiber diameter measurement system which is capable of measuring the fiber diameter during growth with a diameter resolution of 0.01%, an axial resolution of 10 μm, and a measurement rate of 1 kHz.[3] A schematic of the system, which analyzes the scattering pattern of a fiber illuminated by a He–Ne laser, is shown in Fig. 2. Real-time diameter measurement during growth has made possible feedback control of the fiber diameter. Using a simple analog proportional feedback system, we have achieved closed-loop stability of the fiber diameter to better than 0.5% over a length of several centimeters leading us to expect significantly lower losses than in previously grown single-crystal fibers.

We compare measurements on fibers during growth with the predictions of a theory we have developed to model the dynamics of fiber growth and apply these results to the growth of diameter stabilized fibers. We report on measurements of losses in fibers grown under feedback control and on experiments on the intentional modulation of fiber diameter for application to devices such as Bragg mirrors or filters.

The successful demonstration of controlled diameter single-crystal fiber growth should allow application of single-crystal fibers to a variety of optical and nonlinear optical devices such as laser oscillators and amplifiers, electrooptic modulators, and harmonic and parametric generators. (12 min)

1. M. M. Fejer, J. L. Nightingale, G. A. Magel, and R. L. Byer, Rev. Sci. Instrum. (Nov. 1984).
2. C. A. Burrus and J. Stone, Appl. Phys. Lett. 26, 318 (1975).
3. M. M. Fejer, G. A. Magel, and R. L. Byer, to be published.

THH3 Development of single-mode fibers and coherent fiber bundles for CO_2 lasers and forward-looking infrared systems

DAN ROCK, Texas Instruments, Inc., P.O. Box 660246, Dallas, Tex. 75266.

Since 1975, several researchers, including Dianov, Miyashita, LeSargent, Harrington, Hartouni, and Bornstein, have been working on IR transmitting fiber optics for the far-IR (8–12-μm) spectral range. Numerous possible applications are discussed in several articles. The work reported to date has been divided between polycrystalline materials, such as KRS-5 and AgCl, and amorphous materials, such as As_2S_3 and GeAsSe glasses, with a small amount of work done by Israel in $Ge_{28}Sb_{12}Se_{60}$ (TI 1173 glass). Polycrystalline fibers, having absorption levels of <1 dB/m at 10.6 μm, have never been successfully clad by any research group and suffer from several problems such as low strength, thermal instability, aging effects, restrictions on minimum fiber diameters, and the potential for permanent deformation during bending. Chalcogenide glass fibers have been clad using the rod-in-tube approach and the double-crucible method but have higher absorption levels than do polycrystalline fibers. No one since Kapany (late 1960s) has reported producing anything other than single-fiber products for the far-IR region.

One of the two goals of the IR fiber program, begun in Jan. 1983 at Texas Instruments, was to produce a single- clad-fiber product with a flat spectral response approaching 1 dB/m over the entire 8–11-μm spectral range. The other program goal was to produce an image bundle of 3000 to 5000 clad fibers with core diameters of <5 mils (127 μm) operating in the 8–11-μm spectral range. Since no one to date has reported any attempts to fabricate an image bundle operating in this spectral range, expectations of optical performance and problems associated with bundle manufacture were unknown. The emphasis, therefore, was to evaluate the optical performance of IR image bundles and manufacturing problems associated with IR bundle manufacture.

The results of the three-year program to develop IR transmitting fibers for the 8–11-μm spectral range can be summarized as follows:

demonstrated multiple core/clad combinations of GeSbSe-based fibers;

made compressive clad fibers of any size without seriously degrading bulk optical properties in the 6–11-μm spectral range;

identified three impurities in addition to their sources in TI 1173 glass that affect absorption levels and fiber strength;

demonstrated potential of producing single-mode IR fibers with compressive cladding;

demonstrated that GeSbSe-based fibers are amenable to conventional fiber and bundle processing;

made bundles of fibers without devitrification;

surface studies indicate the presence of a 400-Å crust of carbon, oxides, and nitrides and its source;

completed fabrication of a $200K custom IR fiber test bench using internal funds.

Work shifts in 1985 from internal funding to IR&D funds. The emphasis of this work will be in two areas: (1) improving bulk absorption levels by investigating new processing techniques; (2) improving the preform fabrication process to improve fiber quality. (12 min)

THH4 High-performance optical isolator for a wide temperature range using a temperature compensated Faraday rotator

SHIGETAKA MATSUMOTO and SHIZUO SUZUKI, KDD Research & Development Laboratories, 2-1-23 Nakameguro, Meguro-ku, Tokyo, Japan.

Optical measuring systems and optical communication systems often need optical isolators which have large isolation with small insertion loss and which are stable for a wide environmental temperature change. For a wavelength region from 1.3 to 1.55 μm, $Y_3Fe_5O_{12}$ is frequently used for a Faraday rotator. However, its temperature dependence of Faraday rotation is not sufficiently small for the above application. Therefore, we developed an isolator using a Faraday rotator ($Y_{1.7}Gd_{1.3}Fe_5O_{12}$) with excellent temperature characteristics and large isolation.

Figure 1 shows the temperature characteristics of the isolator measured at 1.3 μm. Isolation and insertion loss at 20°C are 40.7 and 1.10 dB, respectively. For a temperature range from 0 to 50°C, the isolation exceeds 40 dB with small degradation. The isolation is improved by reducing light beam size, because it is restricted by the extinction ratio of the rotator, and the ratio decreases with reduction of the beam size. As for the insertion loss, it never exceeds 1.5 dB for the temperature range. Absorption loss of the rotator is only 0.35 dB and increases 0.1 dB at most when temperature varies from 0 to 50°C. Excess insertion loss and its excess increase are both attributed to reflection and absorption loss of two calcite polarizers. Therefore, it can be also reduced to 0.9 dB by applying antireflection coatings to the polarizers.

As mentioned above, the Faraday rotator consists of $Y_{1.7}Gd_{1.3}Fe_5O_{12}$ and a mixed crystal of $Y_3Fe_5O_{12}$ and $Gd_3Fe_5O_{12}$. Temperature characteristics of a few kinds of mixed crystals are shown in Fig. 2. Estimating from the characteristics of $Y_{1.7}Gd_{1.3}Fe_5O_{12}$ and $Y_{1.9}Gd_{1.1}Fe_5O_{12}$ in the figure, the temperature dependence of the Faraday rotation enables isolators using them as rotators to maintain isolation >50 dB, if all the components of the isolator have an extinction ratio of <10^{-5}. On the other hand, it is not possible to obtain such high isolation using $Y_3Fe_5O_{12}$ for the same temperature range, with only 38 dB for $Y_3Fe_5O_{12}$ from the temperature characteristics shown in the figure.

In summary: A high-performance optical isolator with isolation >40 dB and insertion loss <1.5 dB for a temperature range from 0 to 50°C has been developed. (12 min)

THH5 Broadly tunable optical parametric oscillator using the urea crystal

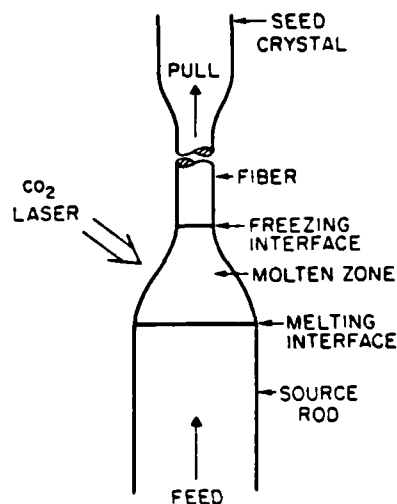C. L. TANG, K. CHENG, M. J. ROSKER, and S. STROBEL, Cornell University, Ithaca, N. Y. 14853.

Recent experiments on optical parametric oscillators[1,2] have shown that these solid-state devices are continuously tunable over rather large tuning ranges.
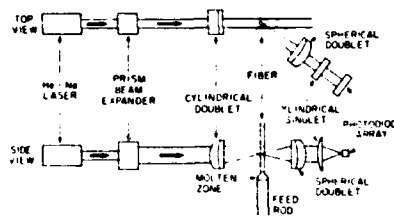
Optical parametric oscillation (OPO) in crystalline urea pumped with the third harmonic (355 nm) of a Nd:YAG laser has earlier been shown to be continuously tunable from 500 nm to 1.22 μm. The efficiency (>20%), linewidth (typically 1.2 Å), spatial mode, and temporal profile of the OPO were characterized and found to compare favorably with other tunable sources at the same wavelength (e.g., pulsed dye lasers). Relatively efficient (>8%) doubling of the output of such an oscillator in a second urea crystal provided for continuously tunable radiation from 250 nm to 1.22 μm. The results of these experiments will be reviewed.

Previous urea OPO experiments made use of a crystal 2.3 cm in length. Because good optical quality urea crystals of this size are still relatively difficult to grow, it is important to demonstrate parametric oscillation in shorter crystals. An OPO with a 1.3-cm long crystal has been constructed and successfully operated. Results obtained from this oscillator will be reported. Urea crystals of this length can be grown much more easily making such an OPO a practical device.
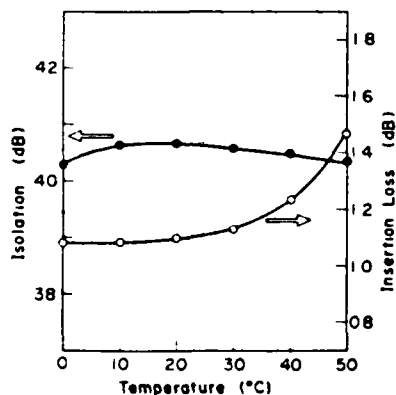
With the fourth harmonic (266 nm) of a Nd:YAG laser output as a pump, a urea OPO utilizing type I phase matching is potentially continuously tunable from 330 nm to 1.4 μm, a very important spectral range. We report the observation of the corresponding parametric fluorescence, and we discuss
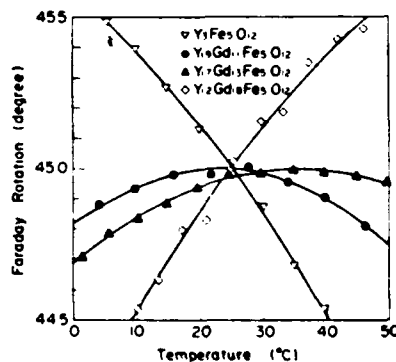
THH2   Fig. 1.   Laser-heated miniature pedestal growth process.

THH2   Fig. 2.   Schematic diagram of the fiber diameter measurement system.

THH4   Fig. 1.   Temperature dependence of isolation and insertion loss of the isolator. Isolation >40 dB and insertion loss <1.5 dB are obtained for a measured temperature range. Beam diameter for 1/e power is ~0.2 mm.

THH4   Fig. 2.   Temperature dependence of Faraday rotation of a few kinds of mixed crystals. Faraday rotation of $Y_{1.7}Gd_{1.3}Fe_5O_{12}$ and $Y_{1.9}Gd_{1.1}Fe_5O_{12}$ is normalized so that the maximum rotation becomes 45°. That of $Y_{1.2}Gd_{1.8}Fe_5O_{12}$ and $Y_3Fe_5O_{12}$ is normalized as it becomes 45° at 25°C.

NONLINEAR OPTICS IN SINGLE CRYSTAL FIBERS

Martin Fejer, John Nightingale, Gregory Magel, William Kozlovsky
Tso Yee Fan and Robert L. Byer
Applied Physics Department
Stanford   University
Stanford, California,   94305

Since the advent of low loss optical fibers fifteen years ago, considerable research effort has been directed towards the study of nonlinear interactions in fibers. A variety of devices have taken advantage of the combination of transverse confinement and long interaction lengths available in glass fibers to operate efficiently at relatively low pump powers. Because glasses are inherently centrosymmetric, only third-order nonlinear processes, e.g. Raman[1] and Brillouin[2] scattering, optical Kerr effect,[3] self-phase modulation,[4] or extremely weak quadrupole second order processes[5] are allowed. Thus, the combination of fiber geometry and the second order susceptibility of non-centro-symmetric single crystals would open the door to a broad range of nonlinear applications not possible in glass fibers.

The potential of crystal fibers for nonlinear interactions is clear from the theoretical efficiencies of several simple devices.[6] A 25 μm diameter 5 cm long $LiNbO_3$ fiber propagating an HE_{11} mode can double 1.06 μm radiation from a Nd:YAG laser with an efficiency of 0.1% per 1 mW or fifty times the bulk efficiency. Similarly, a parametric oscillator pumped with 532 nm radiation in the same fiber would have a threshold on the order of ten mW. The advantage of the guided wave structure is even more pronounced for interactions involving widely disparate frequencies, e.g. differencing two visible lasers to produce infrared radiation, where the advantage relative to the bulk is several hundred to one.

Fibers useful for device applications must meet fairly stringent quality criteria. In order to maintain phasematching in a parametric process and to minimize scatter losses, the fiber must be a properly oriented single crystal of good optical quality and uniform composition. Ferro-electric fibers must, in addition, be poled, i.e. single domain . Diameter variations can cause phase mis-match, radiation losses and modal coupling . These effects are complicated functions of the core-cladding index difference, the radius of the fiber, and the azimuthal and axial period of the variations. We estimate that diameter variations must be held to less than 0.1 - 1% for typical nonlinear devices.

There are a number of research efforts underway to produce non-linear crystal fibers. Organic crystals grown inside glass capillaries are being investigated by several groups.[7,8] These materials exhibit large nonlinear coefficients (in some cases more than an order of magnitude larger than $LiNbO_3$), and high damage thresholds (comparable to KDP). Crystal properties can be tailored to specific applications

by organic synthesis techniques. SHG of a pulsed 1.06 μm laser in a benzil cored fiber was reported several years ago by Nayar.[9] The interaction was quite inefficient because the second harmonic radiation was produced in radiation modes of the fiber.

Another approach to nonlinear interactions in fibers is to embed an unclad glass fiber in a nonlinear crystal. DeShazer has reported promising results in $LiIO_3$ with this technique.[10] His group has also grown KDP crystal fibers by an unspecified method.[11]

The growth technique that we have chosen to pursue is miniature pedestal growth.[12] In this method, the tip of a small rod of the material to be grown is melted with a CO_2 laser, as shown in Fig. 1. A seed crystal is dipped into the molten zone, then pulled from the zone more rapidly than the source rod is fed in. Mass conservation fixes the diameter reduction as the square root of the velocity ratio.

The abrupt liquid solid transition characteristic of the growth of crystalline materials is quite different from the viscous draw-down seen in glass fiber pulling, causing the pedestal growth processes to be far more sensitive than glass fiber pulling to external perturbations. The growth of fibers suitable for nonlinear applications therefore, requires a carefully designed apparatus. In particular, the growth zone must be mechanically and thermally stable and the heat distribution should be azimuthally symmetrical. The apparatus that we designed to meet these criteria is shown in Fig. 2.

The novel reflaxicon focussing system simultaneously provides an azimuthally symmetric heat input and a tight 40 μm focus necessary for the stable growth of small fibers. A moving belt in the translation mechanisms slides the fibers through silicon V-groove guides at rates accurately controlled by regulated d.c. motors. The V-groove guides prevent motion of the fiber in the plane perpendicular to the growth axis. A high speed non-contact diameter measurement system described in detail elsewhere has recently been completed. This device will allow study of the effect of variations of feed and pull rates and laser power on the fiber diameter, with the goal of implementing closed loop control of the fiber cross-section. A block diagram of the complete system is shown in Fig. 3. Reference 12 gives a more complete description of the apparatus.

To date we have achieved controlled growth of four materials: Al_2O_3 , $Cr^{+++}:Al_2O_3$, $Nd^{++}:YAG$ and $LiNbO_3$. Several orientations of most of these materials have been grown, including both a and c axis $LiNbO_3$. Fibers with diameters ranging from 20 up to 500 μm have been grown at rates of 0.5 to 40 mm/min in lengths up to 200 mm. The necessary CO_2 laser power is typically less than 5 W.

The morphology of the fibers is similar to that of bulk Czochralski boules of the same orientation. For example <111> Nd:YAG fibers show a rounded hexagonal shape, while <001> $LiNbO_3$ fibers are round with three growth ridges. SEM photographs of the fibers show no micron scale roughness, but diameter variations on the order of 1% rms are observed over millimeter lengths. We expect to reduce

these variations by an order of magnitude with the closed loop diameter control system.

These growth results illustrate several of the attractive features of the miniature pedestal growth technique. It is entirely containerless, thereby avoiding crucible compatibility and contamination problems. Feasible pull rates are orders of magnitude higher than in bulk Czochralski growth and only small volumes of starting material are required. High temperatures are easily attained, with the available laser power as the only limit. 0.5 mm diameter sapphire (M.P.2323K) can be grown with only 5 watts of laser power. Thus, the technique is attractive for material survey applications, e.g. new laser host-ion combinations.

The measured propagation losses in the fibers are in accord with theoretical estimates based on the measured amplitude of the diameter variations. For example, a 5 cm long 170 μm diameter ruby fiber had losses of 0.04 dB/cm for 633 nm radiation launched into low order modes. Similar results were obtained in Nd:YAG and LiNbO$_3$ fibers.

The first optical device that we have constructed using single crystal fibers is an argon laser pumped monolithic cw ruby fiber oscillator.[14] This device demonstrates the feasibility of monolithic guided wave devices in crystal fibers.

We are currently studying two problems which must be understood before nonlinear devices can be fabricated in LiNbO$_3$ fibers: control of the distribution of ferro-electric domains, and cladding the fiber for control of modal characteristics. Selective etching and pyro-electric response studies indicate the c-axis fibers grow single domain, while a-axis fibers develop head-to-head domains joined at the axis of the fiber. Both these results can be explained by the thermo-electric fields which are present in the growth zone. Generated by the steep temperature gradients present in the pedestal growth process, these electric fields dominate the dipole-dipole interactions that cause bulk samples to break up into polydomain configurations. Efforts are underway to use controlled temperature gradients to uniformly pole a-axis fibers. It may also be feasible to use periodically varying temperature gradients to form a periodically poled fiber for quasi-phasematching[15] nonlinear interactions.

Techniques for forming low index claddings are also being studied. Such claddings would reduce surface scatter losses and bring the waveguides closer to single mode operation. Both extruded glass and diffused proton or transition metal claddings have been fabricated and are being tested.

Conclusions

We have designed and built an apparatus to grow single crystal fibers suitable for linear and nonlinear optical applications. Ruby, lithium niobate and Nd:YAG fibers with losses in the 1%/cm range have been grown. An argon pumped monolithic ruby fiber oscillator has been demonstrated.

Future work will proceed in several directions. Studies of cladding and poling a-axis LiNbO3 will continue. The short term goal is demonstration of efficient doubling of 1.06 μm radiation. The first nonlinear device we expect to demonstrate is an electro-optic modulator in c-axis $LiNbO_3$ as the poling problem is already solved for this orientation.

Another thrust of the program will be extending the range of materials grown in fiber form. Two materials to be emphasized are terbium gallium garnet for optical isolators and potassium niobate for doubling gallium arsenide diode lasers.

References

1. R.H. Stolen, "Fiber Raman Lasers", Fiber and Integrated Optics, 3 (1980).

2. E. Ippen and R.H. Stolen, "Stimulated Brillouin Scattering in Optical Fibers", Appl. Phys. Letts. 21, 539 (1972).

3. V. Dziedzic, R.H. Stolen and A. Ashkin, "Optical Kerr Effect in Long Fibers", Appl. Opt. 20, 1403 (1981).

4. E. Ippen, C. Shank, T. Gustafson, "Self-Phase Modulation of Picosecond Pulses in Optical Fibers", Appl. Phys. Letts. 24, 190 (1974).

5. Y. Ohmori and Y. Sasaki, "Two Wave Sum Frequency Light Generation in Optical Fibers", IEEE Journ. Quant. Electr. QE-18, 758 (1982).

6. M. Fejer, R.L. Byer, "Nonlinear Optics in Single Crystal Fibers", to be published.

7. J. Zyss and J.L. Oudar, "New Organic Molecule Materials for Nonlinear Optics", C.L.E.O.,Anaheim, 1984, Session FO4.

8. B. Nayar, D. Smith, C. Yoon and J. Sherwood, "Growth and Assessment of Highly Nonlinear Organic Materials", C.L.E.O., Anaheim, 1984, Session FO1.

9. B. Nayar, in Technical Digest, Topical Meeting on Integrated and Guided Wave Optics, (O.S.A. Washington D.C, 1982, Paper ThA2.

10. L. deShazer, private communication.

11. Ibid.

12. M. Fejer, J. Nightingale, G. Magel and R.L. Byer, "Laser Heated Miniature Pedestal Growth Apparatus for Single Crystal Optical Fibers", Rev. Sci. Instrum. 55, 1791 (1984).

13. M. Fejer, G. Magel and R.L. Byer, "High Speed, High Resolution, Fiber Diameter Measurement System", Appl. Opt. 24, 2362 (1985).

14. J. Nightingale, R.L. Byer, "A Guided Wave Monolithic Ruby Fiber Laser", to be published.

15. J.D. McMullen, "Optical Parametric Interactions in Isotropic Materials Using a Phase Corrected Stack of Nonlinear Dielectric Plates", J. Appl. Phys. 46, 3076 (1975).
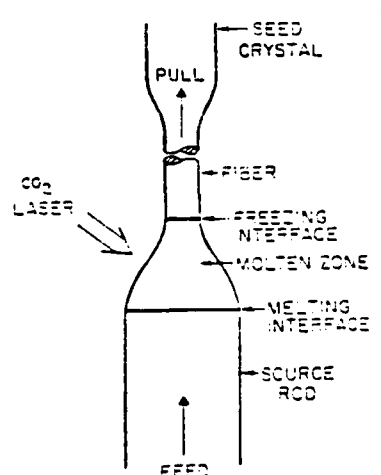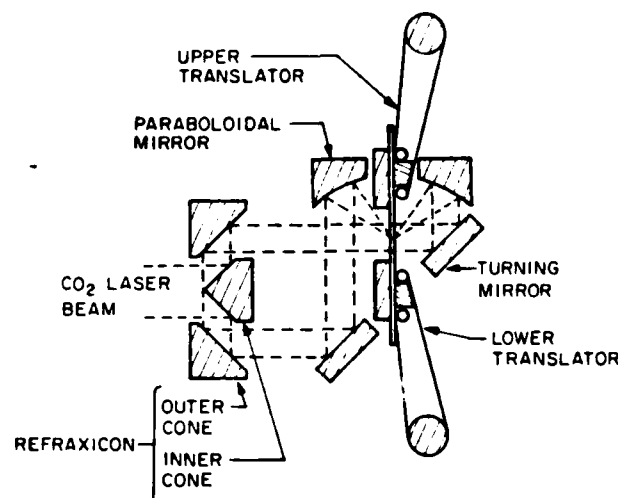
Fig. 1
The laser heated miniature pedestal growth process.

Fig. 2
CO_2 laser focusing optics and fiber translation system.

Fig. 3--Block diagram of the single crystal fiber growth system

Characterization of proton-exchanged waveguides in MgO:LiNbO₃

M. Digonnet, M. Fejer, and R. Byer

Edward L. Ginzton Laboratory, W. W. Hansen Laboratories of Physics, Stanford University, Stanford, California 94305

We report the fabrication and characterization of proton-exchanged waveguides in MgO-doped LiNbO₃, a high-optical-damage-threshold material. Results indicate waveguide characteristics similar to those of waveguides fabricated in undoped LiNbO₃ except for slower diffusion rates and freedom from etching of the y face when pure benzoic acid is used as a proton source. An optical-damage threshold of 70 kW/cm² was measured at 0.5145 μm in a MgO:LiNbO₃ waveguide, corresponding to a factor-of-2 improvement over undoped LiNbO₃.

It was shown by Zhong et al.,[1] and more recently by Bryan et al.,[2] that LiNbO₃ doped with approximately 5% or more MgO exhibits a remarkably reduced photorefractive response compared with undoped LiNbO₃. It is believed that the reduced photorefractive response is due to the increased photoconductivity of the MgO:LiNbO₃.[2] Such a material offers great promise for nonlinear and integrated optics, for which induced photorefractivity (optical damage) has been a serious limitation in the past. It must be noted that the enhanced photoconductivity may cause deleterious effects in devices requiring the application of low-frequency electric fields.

As a first step toward the demonstration of efficient nonlinear guided-wave devices, it was interesting to fabricate proton-exchanged waveguides in MgO:LiNbO₃. Compared with other waveguide fabrication processes in LiNbO₃, proton exchange has been shown to be a rapid low-temperature process and to yield waveguides with interesting applications in polarization filtering and birefringence control.[3] In this Letter we report the fabrication of H⁺-exchanged waveguides in MgO:LiNbO₃ and describe the waveguide characteristics and power handling at short wavelengths.

Waveguides were fabricated in x- and y-cut 5% MgO-doped LiNbO₃ crystals grown by Crystal Technology, Palo Alto, California. The now standard technique of proton exchange in a melt of benzoic acid containing varying amounts of lithium benzoate was used.[4,5] Benzoic acid has been shown to have an appropriate dissociation constant, melting temperature, and stability as a liquid for use in this process.[3,4] The addition of lithium benzoate to the melt provides a means of controlling the proton concentration in the exchanged region, which has a strong bearing on the crystal structure and the optical properties and quality of the waveguide.[6]

The acid melt, containing between 0 and 2 mol % lithium benzoate, was contained in a glass flask equipped with a condensing column. The column was used to reduce material loss and composition change of the melt, as the waveguide characteristics have been

shown to depend strongly on the concentration of Li⁺ ions in the melt.[4] The wafer to be exchanged was held in a glass tube provided with lateral cuts to let the liquid penetrate inside the tube. All exchanges were performed at the boiling temperature of the melt, about 249°C in pure acid and 246 and 243°C for melts containing 1 and 2% lithium benzoate, respectively. This arrangement yielded easily reproducible results.

After fabrication the waveguide index profiles were characterized using the prism-coupling launching-angle measurement to determine the effective indices of the guided modes. The guide index profile was then recovered from the mode indices with a standard inverse WKB method. Figure 1 shows a typical set of index profiles measured at different wavelengths for an x-cut MgO:LiNbO₃ waveguide exchanged for 3 h in pure benzoic acid. The profiles exhibit the same step-index shape as is characteristic of proton-exchanged waveguides in undoped LiNbO₃ with an increase of the ex-
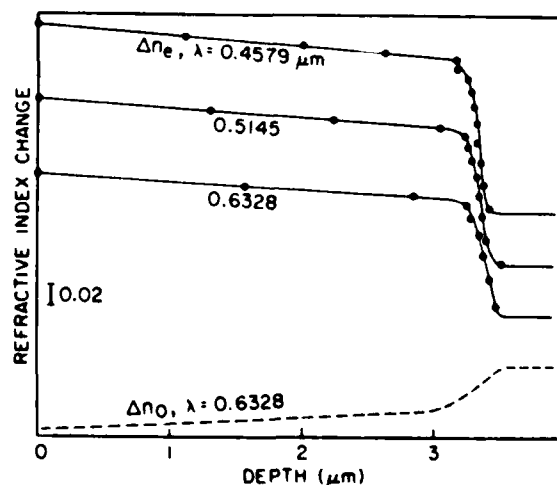

Fig. 1. Typical n_e and n_o profiles of a proton-exchanged waveguide in MgO:LiNbO₃. The x-cut wafer was processed for 3 h in pure benzoic acid at 245°C. The profiles were shifted vertically for clarity.
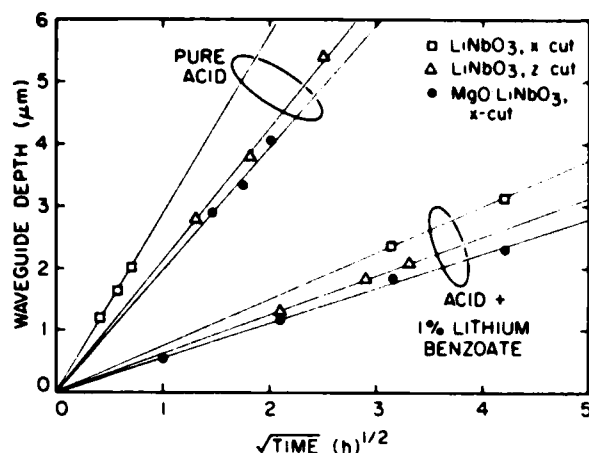
Fig. 2. Waveguide depth versus the square root of the exchange time in doped and undoped LiNbO₃ treated in melts of different compositions.

traordinary index (of the order of 0.135 at the wavelength of $\lambda = 0.6328\ \mu$m) and a decrease of the ordinary index. This result indicates that the presence of MgO in the crystal lattice does not significantly alter the exchange process.

The negative ordinary index profile was measured by launching a wave at an angle θ to the usual propagation direction (along y) in an x-cut waveguide. The resulting index step Δn seen by the wave is then a known combination of Δn_e and Δn_o, from which the latter can easily be extracted. Alternatively, one can measure the critical angle θ_c for which the wafer no longer supports a guided mode. This method yielded the value of $\Delta n_o = -0.06 \pm 0.006$, in good agreement with previously published values for the undoped material.[4]

We show in Fig. 2 the evolution of the waveguide depth with the square root of the exchange time for waveguides fabricated in MgO-doped and -undoped LiNbO₃ in melts of different compositions. The dependence is linear, which suggests a diffusionlike behavior for both materials. One can thus characterize the exchange rate by the diffusion coefficient D, defined by[3] $d = (4Dt)^{1/2}$, where d is the depth (at half-maximum) of the waveguide and t the exchange time. As is shown in Fig. 3, the exchange rate decreases as the Li⁺ melt concentration is increased, following an exponential law previously established for undoped LiNbO₃.[7] The exchange rate is lower in z-cut than in x-cut wafers for the undoped material, and is even lower in the x-cut orientation for the doped material. This result is similar to the situation in Ti-diffused LiNbO₃, where the presence of Ti slows down the proton-exchange rate.[8] Note that the exchange rate is still very high with melts containing up to 1% of lithium benzoate; a single-mode waveguide can be fabricated in less than a few minutes.

Waveguides were also fabricated in y-cut MgO: LiNbO₃ in pure benzoic acid with no evidence of surface etching up to the maximum exchange time that was tested, about 4 h. Again, this observation parallels that of other authors concerning proton exchange in waveguides previously doped with titanium.[8] The diffusion

rates were found to be essentially the same for x-cut and y-cut MgO:LiNbO₃.

Figure 4 illustrates the index changes Δn_e measured in two MgO:LiNbO₃ waveguides at different wavelengths and the corresponding single-pole Sellmeier curve to which they were fitted. The index change was found to vary substantially across the visible and near-infrared ranges, from about 0.18 at 0.4579 μm to 0.12 at 0.820 μm for waveguides made in pure acid. This fairly strong Δn_e dispersion indicates a higher index dispersion for $Li_{1-x}H_xNbO_3$ (whether or not doped with MgO) than for unexchanged LiNbO₃ for the wide range of proton concentration x that was tested. For a given Li concentration, we found that Δn_e was larger in the doped than in the undoped material by about 2–3×10^{-3} for x-cut samples. Δn_e decreases linearly with increasing Li concentration in the melt, with essentially the same slope for the MgO-doped (x-cut) and undoped (x and z cuts) material. We measured a slope $d(\Delta n_e)/d[L_1^+]$ of -0.019/mol % at $\lambda = 0.6328\ \mu$m

Several authors reported aging of proton-exchanged LiNbO₃ waveguides, apparent as a reduction of the surface index and of the waveguide depth over a period of a few days, especially in waveguides fabricated in pure acid.[7] The same phenomena were observed in H⁺: MgO:LiNbO₃ waveguides. Stronger mode coupling was also noticed in waveguides exchanged in pure acid. Postannealing, a process that was shown to eliminate these difficulties,[7] is clearly also needed for doped LiNbO₃ to control the crystal phase of the exchanged layer and stabilize its surface index. Since we did not anneal our waveguides after exchange, we performed all the measurements described here approximately one day after the wafer was removed from the melt to keep our results consistent.

Zero-field photorefractive sensitivity (optical damage) in both types of waveguides was observed to have a fairly high threshold at short wavelengths. Up to about 1 mW of light was coupled into our waveguides for routine characterization without apparent long-term effects on the waveguide index, even at 0.4579 μm.

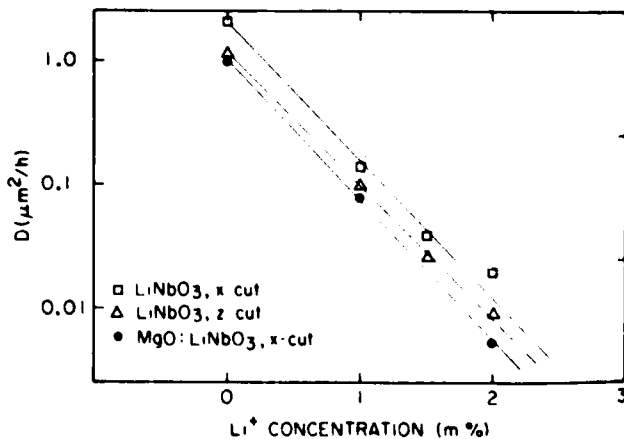Fig. 3. Comparison of proton-diffusion rate in doped and undoped LiNbO₃ as a function of the Li⁺ concentration in the melt.
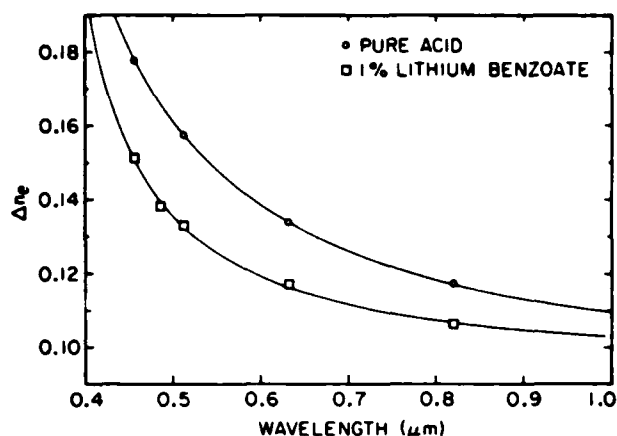
Fig. 4. Δn_e dispersion of x-cut MgO:doped LiNbO$_3$ wave-guides for two Li$^+$ concentrations in the melt.

Quantitative measurements also indicated a good short-term tolerance to relatively high optical intensities.   Short-term optical-damage thresholds were measured by prism coupling a 0.5145-μm beam focused in the waveguide plane to a 40-μm-diameter spot size with a cylindrical lens. The TE$_0$ mode output was apertured with a narrow slit and recorded as a function of time for different power levels. Damage appeared as a broadening of the output mode in the plane of the waveguide and was recorded as a drop of the measured power. The short-term-damage threshold was arbitrarily defined as the coupled power at which the recorded output dropped by 10% in 1 min. Damage thresholds were slightly higher in annealed samples (annealing was performed by bringing the wafers up to about 250°C and letting them cool slowly over several hours). Initial measurements indicate a threshold of 13 mW in a nine-mode undoped LiNbO$_3$ waveguide and 10.5 mW in a three-mode MgO:LiNbO$_3$ waveguide. This corresponds to an intensity of 35 and 70 kW/cm^2, respectively, one of the highest intensities achieved to date in a LiNbO$_3$ waveguide at this wavelength and about 4 orders of magnitude higher than we observed in Ti-diffused LiNbO$_3$ guides.

It should be noted that the photorefractive sensitivity of a LiNbO$_3$ waveguide is a complicated function of the optical and thermochemical history of the device. The simple test described here is useful for the comparison of short-term damage effects in various waveguides, but it must be recognized that more-sensitive measurement techniques[9] would undoubtedly find damage effects at intensities much lower than those reported here.

It was recently reported that proton-exchanged waveguides in undoped LiNbO$_3$ have significantly increased dark conductivity. This enhanced dark conductivity probably accounts for the relatively small advantage of highly photoconductive MgO:LiNbO$_3$ over the undoped material for proton-exchanged waveguides.[10] Further tests are now under way to improve the power tolerance of the waveguides.

In conclusion, we have characterized the parameters of proton-exchanged waveguides in high-damage-threshold MgO:LiNbO$_3$ and have compared these with waveguides made in undoped LiNbO$_3$. The major differences include a slower proton-diffusion rate and no etching of the y face in MgO:LiNbO$_3$ waveguides, as has also been observed in Ti-diffused, proton-exchanged waveguides. A factor-of-2 improvement in optical damage threshold (about 70 kW/cm^2) at 0.5145 μm was achieved in a proton-exchanged MgO-doped LiNbO$_3$ waveguide compared with a waveguide made of undoped LiNbO$_3$.

References

1. G.-G. Zhong, in *Proceedings of 11th International Quantum Electronics Conference*, IEEE catalog no. 80, CH1561-0 (Optical Society of America, Washington, D.C., 1980), p. 631.

2. D. A. Bryan, R. Gerson, and H. E. Tomaschke, Appl. Phys. Lett. 44, 847 (1984).

3. J. L. Jackel, C. E. Rice, and J. J. Veselka, Appl. Phys. Lett. 41, 607 (1982).

4. M. DeMicheli, J. Botineau, S. Neveu, P. Sibillot, D. B. Ostrowsky, and M. Papuchon, Opt. Lett. 8, 114 (1983).

5. J. L. Jackel, C. E. Rice, and J. J. Veselka, Electron. Lett. 19, 387 (1983).

6. C. E. Rice and J. L. Jackel, Mat. Res. Bull. 19, 591 (1984).

7. J. L. Jackel and C. E. Rice, Proc. Soc. Photo-Opt. Instrum. Eng. 460, 43 (1984).

8. M. DeMicheli, J. Botineau, P. Sibillot, D. B. Ostrowski, and M. Papuchon, Opt. Commun. 42, 101 (1982).

9. R. A. Becker, Soc. Photo-Opt. Instrum. Eng. 460, 95 (1984).

10. R. A. Becker, Proc. Soc. Photo-Opt. Instrum. Eng. 517, 194 (1984).

Processing of Guided Wave Optoelectronic Materials

January 24–25, 1984
Los Angeles, California

Laser assisted growth of optical quality single crystal fibers

M. M. Fejer, J. L. Nightingale, G. A. Magel, R. L. Byer
Applied Physics Department, Stanford University, Stanford, California 94305

Laser assisted growth of optical quality single crystal fibers

M.M. Fejer, J.L. Nightingale, G.A. Magel and R.L. Byer

Applied Physics Department, Stanford University, Stanford,
California 94305

Abstract

Single crystal fibers of four refractory oxide materials (Al_2O_3 , $Cr:Al_2O_3$, Nd:YAG and $LiNbO_3$) have been grown by a miniature pedestal growth technique. The growth apparatus employs novel electronic control, mechanical and optical systems enabling growth of high optical quality fibers. All four materials exhibit similar growth characteristics and yield fibers of comparable quality. Measured optical waveguide losses at 632.8 nm for a 5 cm long 170 μm diameter $Cr:Al_2O_3$ fiber were 0.04 dB/cm.

Introduction

The ability to fabricate optical waveguides in materials other than glass offers new and interesting device opportunities. In particular, waveguides formed from single crystal fibers offer the potential to make devices that utilize the unique optical and nonlinear optical properties of single crystals in a guided wave structure.

In this paper we report the growth of single crystal fibers using a laser assisted miniature pedestal growth technique.[1,2,3] To implement the growth of small diameter, oriented, single crystal fibers, we have designed and constructed a fiber growth apparatus that uses a waveguide CO_2 laser source and a unique symmetrical optical focusing system.[4,5]

The advantages of single crystal fibers are best illustrated by considering potential applications. The applications, in turn, generate a set of criteria that the single crystal fibers must meet if they are to be useful in devices. Following the discussion of applications and fiber parameters, we describe the growth apparatus and recent growth results . We then review optical measurements of single crystal fibers and summarize progress toward single crystal fiber devices.

Applications and properties of single crystal fibers

The growth of single crystal fibers is motivated by their application to linear and non-linear optical devices that are not possible in glass fibers. For convenience, we classify devices as passive, active and nonlinear. Table I lists examples of possible single crystal fiber applications within these classes and illustrates each application area by some representative materials. In addition to device applications, the rapid growth of single crystal fibers makes them useful for material surveys.

Table I. List of 4 different classes of applications and some specific devices in each class. Some representative crystalline materials for each application are given in the right hand column.

Passive Devices	
Lightguide	Al_2O_3
Thermometer	
Polarizer	
Active Devices	
Laser amplifier	Nd^{+++}:YAG
Laser oscillator	Cr^{+++}:Al_2O_3
	Ti^{+++}:Al_2O_3
Nonlinear Devices	
Modulator	$LiNbO_3$
Mixer	
Harmonic generator	
Parametric oscillator	
Materials Surveys	
Laser host-ion combinations	$Ti:Al_2O_3$

To date we have grown single crystal fibers of Al_2O_3 , Cr^{+++}:Al_2O_3 , Nd^{+++}:YAG and $LiNbO_3$, in the orientations, lengths, and diameters shown in Table II.. This list is representative and not intended to be complete, since more than thirty materials have been grown by this technique at Stanford University.[6]

The optical attenuation of a single crystal fiber is determined by a number of factors including crystal defects, impurity concentration, compositional inhomogenieties and diameter fluctuations.

Fiber diameter control is of concern since random diameter fluctuations of only 1% can lead to modal conversion and scatter losses in the range of 5% cm^{-1}. However, for a typical case, diameter fluctuations of 0.1% yield calculated losses of only .05% cm^{-1}. Periodic diameter modulation of the fiber also leads to scatter losses. However, if properly controlled, periodic fiber diameter modulation may be useful as a Bragg mirror or filter.

Table II. Representative Single Crystal Fibers

Material	Orient- ation	Length (cm)	Diameter (μm)
$A\ell_2O_3$	<001>	20	170
		3.5	50
$A\ell_2O_3$ + 0.05 wt % Cr	<001>	10.0	170
		3.0	95
YAG + 0.9 wt % Nd	<111>	3.5	110
$LiNbO_3$	<001>	3.5	50
	<100>	3.0	170

The optical loss resulting from diameter variations can be reduced by using a diffused cladding if the diffusion depth is large compared to the scale length of the diameter variations. Such a cladding might be achieved in $LiNbO_3$ by diffusing protons into the fiber using known techniques.[7]

To date fibers grown with our apparatus have shown diameter fluctuations on the order of several percent under open loop growth conditions. We have designed and plan to implement closed loop diameter control during fiber growth using a novel diameter measurement apparatus.[8] Fiber diameter uniformity of 0.1% should be achieved using this system.

The device applications of single crystal fibers shown in Table I determine the fiber parameters necessary for good device performance. Important crystal fiber parameters include length, diameter, and optical loss. Table III summarizes typical single crystal parameters required for thermometry using an $A\ell_2O_3$ fiber[9] and for second harmonic generation using a $LiNbO_3$ fiber.

Table III. Typical single crystal fiber parameters for device applications

Passive device
(Thermometry using sapphire)
- length   - 20 cm
- diameter   - 70 microns
- diameter variations - 1%

Nonlinear device
(SHG using lithium niobate)
- length   - 5 cm
- diameter   - 25 microns
- diameter variations - 0.1%
- efficiency   - 0.1%/mW

High temperature thermometry is possible using blackbody emission guided along a sapphire fiber. Since the sapphire fiber can be optically coupled to a glass fiber only the portion of fiber exposed to high temperatures need be sapphire. We thus anticipate relatively short, e.g. 20 cm, fiber lengths to be useful. Constraints on fiber flexibility generally determine the maximum allowable fiber diameter. A 70 μm diameter sapphire fiber can be readily bent on a 1 cm radius of curvature, adequate for most applications.

This device is not particularly sensitive to optical loss or mode coupling within the fiber. The allowable diameter variations are, therefore, relatively loose, on the order of 1%.

To date high temperature sapphire thermometry has made use of short sapphire rods coated with iridium metal at the tip.[9] Recently we have grown 170 μm diameter fibers of sapphire up to 20 cm in length for this application. We have also successfully doped the end of the sapphire fiber with metal to provide an integral, stable, blackbody source. Tests are now in progress to demonstrate the use of sapphire fibers as a flexible, high temperature, high speed thermometer.

Nonlinear devices using crystal fibers promise higher frequency conversion efficiency than conventional devices since fibers allow a tight beam confinement over a long interaction length. For example a 5 cm long 25 μm diameter $LiNbO_3$ fiber offers a factor of 50 efficiency improvement compared to second harmonic generation in a bulk crystal. Since this device requires low loss single mode optical propagation in the fiber, the diameter control tolerances are tight, on the order of 0.1%. Thus high conversion efficiency is possible with incident powers on the order of 100 mW, which is the power level now available in single mode diode laser sources.

Crystal growth apparatus

We have designed and built a growth apparatus to produce single crystal fibers of the quality required for device applications. The apparatus uses a laser heated miniature pedestal growth technique first applied to optical fiber growth by Burrus and Stone.[2] Figure 1 illustrates growth of a single crystal fiber using the laser heated miniature pedestal growth technique.

A waveguide CO_2 laser is focused onto the molten zone by a combination refraxicon/ parabolic mirror optical system shown schematically in Fig. 2. A source rod is translated into the focused laser beam via a belt drive translation system. The source rod may be
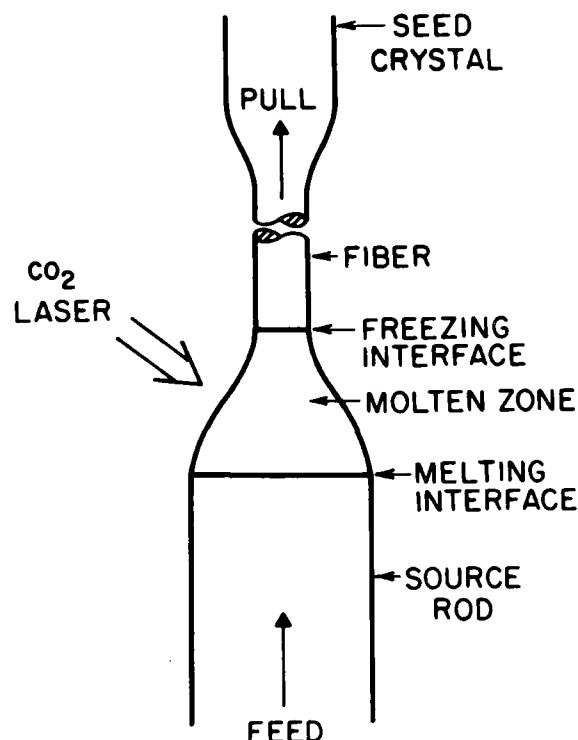
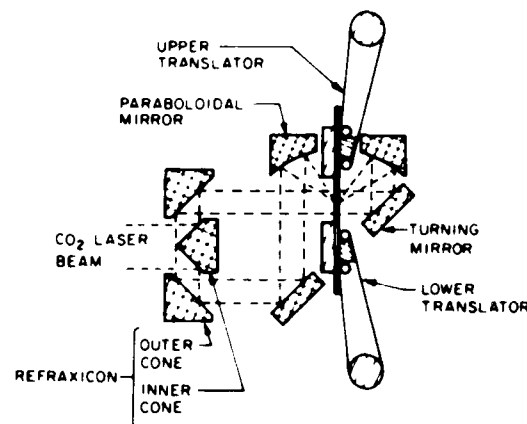Figure 1. Schematic of miniature pedestal growth.

Figure 2. Schematic of focusing system and fiber translation devices.

fabricated from either single crystal, polycrystalline, or hot pressed powder material.

To initiate growth an oriented seed rod is dipped into the molten zone. The seed rod defines the crystallographic orientation of the fiber. Growth proceeds by simultaneously translating the lower and upper fiber source and seed rods. Conservation of mass determines the fiber diameter reduction as the square root of the feed rate to pull rate ratio. Diameter reductions of $3:1$ are typical. Greater diameter reductions are difficult due to the onset of growth instabilities.

Miniature pedestal growth differs from the viscous drawdown of a glass fiber since, unlike glass, crystals have a definite solid/liquid phase transition. The molten zone is a true liquid being held in place by surface tension.

In order to achieve a stable fiber diameter, stable fiber growth conditions must be realized. This in turn dictates a stable mechanical apparatus, smooth feed and pull rates, stable laser power and symmetric heat input into the molten zone.

The optical system shown schematically in Fig. 2 uses copper mirrors to focus the CO_2 laser source onto the molten zone. The refraxicon, in combination with the $f/2$ focusing parabolic mirror, yields a symmetric focus with a 30 μm diameter. The tight focus allows the growth of small diameter fibers.

The translation system shown in Fig. 2 uses a seamless-belt drive system driven by a phaselocked dc motor. The fiber is held in a 'V-groove' etched in a silicon substrate that is oxidized to form a hard silicon dioxide surface. This drive system is in turn controlled by a digital logic system that allows control of the growth rate and diameter reduction ratio.

The present growth apparatus yields fibers with 2% diameter variations over centimeter lengths. The growth of more uniform fibers will require active control of the fiber diameter during growth. Figure 3 shows a schematic of the fiber growth apparatus including a fiber diameter measurement and control system. Since no commercial fiber diameter system met our sensitivity, speed, and working distance requirements, we have designed and built the non-contact diameter measurement system shown in Fig. 4.

The fiber diameter measurement system uses a helium-neon laser to illuminate the fiber. The beam is tightly focused using a cylindrical lens to define the measurement zone along the fiber. In the other plane the beam is scattered by the fiber and imaged onto a
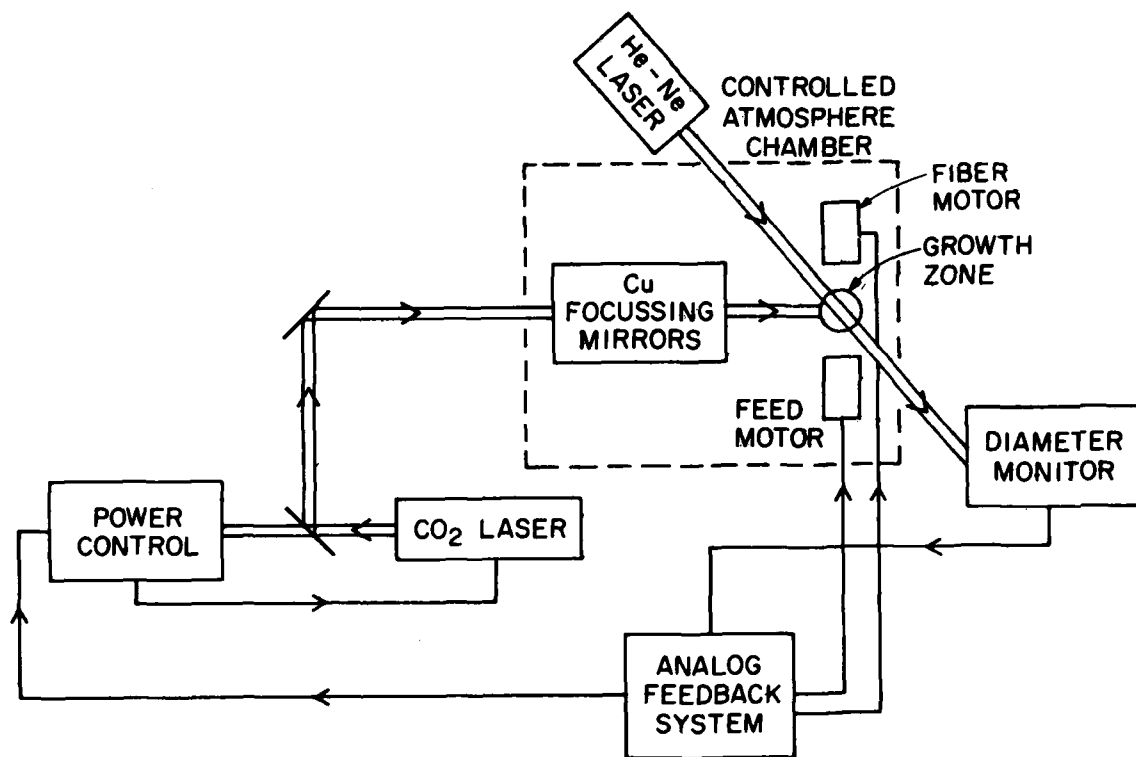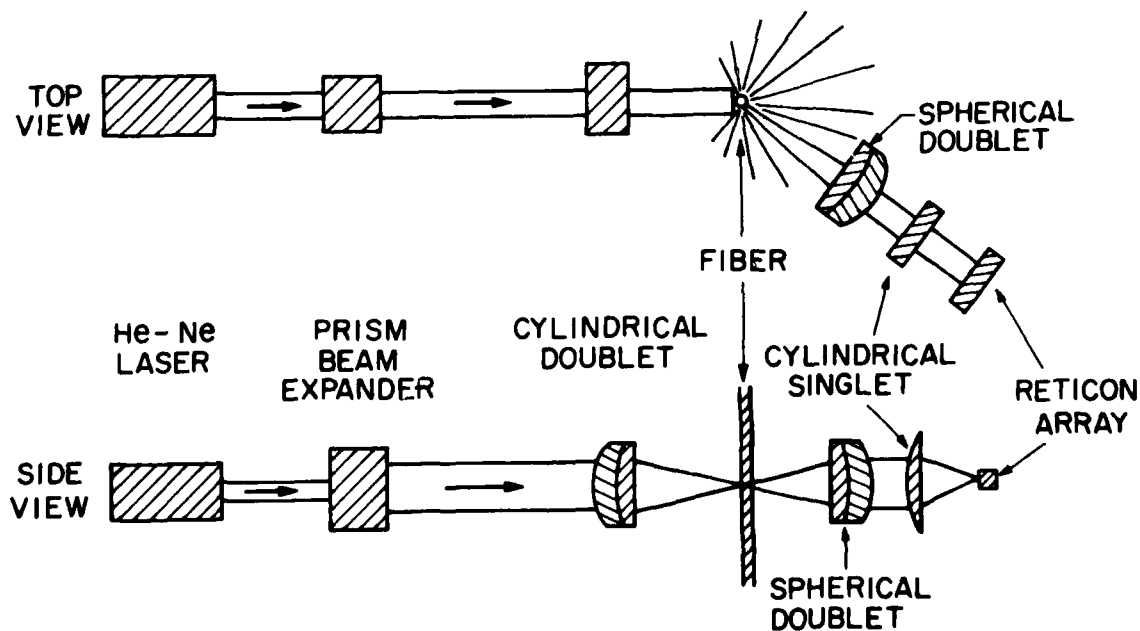
Figure 3. Schematic of fiber growth apparatus.

Figure 4. Schematic of diameter measurement system.

a photodiode array where interference fringes are detected.[10] The interference pattern is analyzed to provide an output signal proportional to the fiber diameter. Recent measurements have shown that the diameter sensitivity is ± 500 Å at a measurement rate of 1 kHz.

The diameter measurement system has not yet been incorporated into the growth apparatus. Thus all fibers grown to date have been without diameter feedback control.

Fiber growth results

In the six months that the fiber growth apparatus has been operational four crystalline materials have been grown: sapphire, ruby, Nd:YAG and LiNbO$_3$. Table II summarizes the length, diameter and orientation of the single crystal fibers. We initiated our growth studies by concentrating on sapphire and chromium doped sapphire or ruby because of availability and ease of growth. Experience with sapphire has enabled us to extend growth studies to Nd:YAG and to LiNbO$_3$. To date we have grown both a-axis and c-axis LiNbO$_3$ with diameters as small as 50 µm and lengths to 3.5 cm.

Typical fiber growth rates range between 1 and 10 mm/min. While these growth rates are slow compared to glass fiber pulling rates, they are orders of magnitude faster than bulk crystal Czochralski growth rates. Since fiber lengths of 5 cm are adequate for many applications useful fiber lengths can be grown in approximately twenty minutes.

The growth apparatus is designed to yield fiber diameters of between 500 and 20 µm. However, smaller diameter fibers to 6 µm have been grown under special circumstances.[6] The initial feed rods are fabricated to 500 µm diameter using a centerless grinder. Diameter reductions of 3 to 1 are normally used during growth. Smaller diameter fibers are grown using previously grown fibers as source rods. The CO_2 laser power required to grow Al_2O_3 and LiNbO$_3$ fibers from 500 µm diameter feed rods are 4.8 and 1.5 watts respectively. The difference is chiefly due to the different melting temperatures of the materials, 2045°C for sapphire and 1260°C for LiNbO$_3$. The required laser power reduces to less than 1 W for fibers grown from 170 µm diameter feed rods.

Sapphire, Nd:YAG and LiNbO$_3$ all display similar growth characteristics. Figure 5 shows the molten zone shape for Al_2O_3. The molten zone shape is similar for the other materials. For optimum growth stability the laser power is adjusted to yield a molten zone with a height-to-width ratio of near unity for a 3 : 1 diameter reduction ratio.

The single crystal fiber growth morphology is similar to that seen in bulk Czochralski growth. For example, <111> axis Nd:YAG fibers show a slightly rounded hexagonal cross-section as shown in Fig. 6. LiNbO$_3$ grown along the optic axis shows a characteristic 3-fold symmetry with growth ridges running parallel to the crystal length as shown in Fig.7 .

Figure 5. Photomicrograph showing growth of a 170 µm diameter Al_2O_3 fiber from a 500 µm diameter source rod. The growing fiber is invisible since its smooth sides scatter very little light.

Figure 6. Scanning electron microscope photograph of cross-section of Nd:YAG fiber.

Figure 7a. Scanning electron microscope photograph of cross-section of LiNbO$_3$ fiber showing pronounced 3-fold growth ridges. The internal concentric ring pattern and dark central area are artifacts of the procedure used to obtain the cross-section.

Figure 7b. Scanning electron microscope photograph of surface of a LiNbO$_3$ fiber. Note the sharply defined growth ridges at the right boundary and near the left edge.

Since the fiber cross-section is invariant with length, the growth morphology should not be detrimental to optical applications.

Early single crystal fibers showed fine scale diameter fluctuations along the fiber length with a scale of 1 - 10 μm.[4] Crystals grown with the current machine are free of these irregularities as shown in Fig. 7b. At a longer length scale we have demonstrated diameter stability to 2% over fibers several centimeters in length.

Optical measurements

We recently have initiated optical property measurements on single crystal fibers. For example, we have measured an optical waveguide loss of 0.04 dB/cm at 632.8 nm in a 5 cm long 170 μm diameter ruby fiber. Comparable losses have been measured in other fibers. For these measurements the single crystal fibers were not cladded so that guiding was provided by the crystal-air dielectric interface. We anticipate lower propagation losses as we grow improved optical fibers and employ more refined cladding techniques.

Sapphire fibers as now grown are suitable for some light-guide applications such as thermometry. For example, we have demonstrated optical propagation in a sapphire fiber heated to 1500°C with no significant change in transmission at the elevated temperatures.

Summary

In summary we have designed and built a fiber growth apparatus to produce high quality single crystal fibers. The apparatus uses the miniature pedestal growth technique which permits the growth of crystal fibers in a wide range of materials. The apparatus is designed to handle fiber diameters as small as 20 microns with fiber lengths exceeding 20 cm. Diameter stability to 2% has been demonstrated over fiber lengths of several centimeters. The optical attenuation of these fibers is 0.04 dB/cm. These fibers are of sufficient quality for simple passive device applications such as high temperature thermometry.

A fiber diameter measurement system has been built which when installed in the growth apparatus should improve the diameter stability and the optical attenuation by an order of magnitude. We anticipate these fibers will be of sufficient quality for a host of active and nonlinear device applications.

Acknowledgements

References

1.   Haggerty, J.S., N.A.S.A. Cr-120948, 1972.
2.   Burrus, C.A., and Stone, J., Appl. Phys. Letts. 26, p.318 (1975).
3.   Stone, J., and Burrus, C.A., Fiber and Integrated Optics, 2, p.19 (1979).
4.   Fejer, M., Byer, R.L., Feigelson, R.S., and Kway, W., Proceedings of the S.P.I.E. Advances in Infrared Fibers II, p.320 (1982).
5.   Fejer, M.M., Nightingale, J.L., Magel, G.A., Byer, R.L., to be published.

6.   Feigelson, R.S., Proceedings of the Fifth International Summer School on Crystal Growth, Davos, Switzerland, 1983.
7.   Jackel,J.L., Rice, C.E., and Vaselka, J.J. Jr., Appl. Phys. Letts. 41, p.607 (1982).
8.   Fejer, M.M., Magel, G.A., and Byer, R.L., to be published.
9.   Dils, R.R., J. Appl. Phys. 54, p.1198 (1983).
10.   Smithgall, D.H., Watkins, L.S., and Frazee, R.E. Jr., Applied Optics, 16, 2395 (1977).

END

DTIC

9 — 86